AD-A235 591

‖‖‖‖‖‖‖‖‖‖‖‖‖‖‖‖
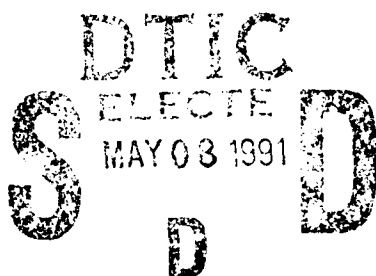
Three Dimensional Analysis of Crack Trapping and Bridging by Tough Particles

M. Ortiz
Division of Engineering
Brown University
Providence, Rhode Island 02912
U.S.A.

91 5 06 126

1. Introduction

Ceramics have several properties that make them appealing materials for a wide range of practical applications. Since their strength is limited by brittle failure, the fracture of ceramics has been the subject of extensive research. However, despite recent progress in the area, a number of issues remain unresolved. For example, while the measured toughness of single crystals is comparable to their surface energy, that of polycrystalline materials is found to be up to an order of magnitude greater. In addition, the apparent toughness of the material is observed to increase with crack length. Three mechanisms have been proposed that may explain this behaviour: crack tip shielding by microcracking; crack deflection; and crack trapping combined with crack face bridging by tough particles.

The possibility that microcracking may improve toughness has recently been the subject of intense investigation. Extensive microcracking is in fact observed around the tips of cracks in brittle polycrystalline materials (Hoagland et al, 1973; Claussen, 1976; Mecholsky et al, 1976; Wu et al, 1978). The microcracks increase the compliance of the solid, and so shield the crack tip from remote stresses. It has been estimated that for a stationary mode I crack, the near-tip stress intensity factors are reduced by around 30% due to microcracking. (Green et al, 1973; Hoagland et al, 1980; Evans and Faber, 1981; Evans, 1984; Evans and Fu, 1985; Kachanov, 1986; Hutchinson, 1987; Rodin, 1987; Ortiz, 1987, 1988; Ortiz and Giannakopoulos, 1989). The effect is slightly greater for a propagating crack, due to the influence of the microcracked wake. (Charalambides and McMeeking, 1987; Ortiz and Giannakopoulos, 1989). However, for a crack in mixed mode or mode II, the shielding effect is almost imperceptible (Ortiz and Giannakopoulos, 1989). Furthermore, although the microcracks do shield the crack tip, they also weaken the material ahead of the crack. Ortiz (1988) has estimated that the reduction in strength due to microcracking almost exactly offsets any gain in toughness due to crack tip shielding. Microcracking does not therefore appear to be an effective toughening mechanism.

Crack deflection is a second plausible mechanism for toughening brittle materials. Since the fracture of ceramics is predominantly intergranular, cracks tend to follow a tortuous path through the material. Second phase particles and inter-granular residual stresses also tend to deflect the path of a crack. This increases the fracture surface area, and consequently raises the apparent toughness of the material. A rigorous three-dimensional analysis of crack deflection has not been attempted to date, but preliminary estimates suggest that crack deflection may increase toughness by around 10–20% (Faber and Evans, 1983, Suresh, 1985).

Crack trapping and crack face bridging are by far the most effective toughening mechanisms. Several experiments have demonstrated that if small quantities of ductile particles are added to a brittle matrix material, its toughness may be increased by up to 60 times (Mendelson and Fine, 1974; Krstic et al, 1981). It has long been recognised that crack bridging is responsible for improving the toughness of fibre-reinforced ceramics and cement. Bridging particles have also been observed in the wake of cracks in monolithic ceramics (Swanson et al, 1987). Fig. 1 illustrates the mechanism for forming bridging particles in the wake of a crack. As a semi-infinite crack propagates through a material containing a distribution of particles, parts of the crack front reach the regions of higher toughness and consequently arrest. As the load is increased, the remainder of the crack continues to propagate, and bows out between the pinning particles. This process of crack trapping is an important source of toughness in itself (Lange, 1970). If the particles are sufficiently tough, the crack front eventually bypasses the obstacles, so that they are left behind in the wake of the crack.

While the origin of bridging particles in composite materials is obvious, it is not immediately apparent why bridging particles should be observed in monolithic ceramics. Evans et al (1977) have suggested that the bridging particles may be attributed to the action of inter-granular residual stresses. Substantial residual stresses may be set up in polycrystalline ceramics during manufacture, due to the thermal and elastic anisotropy of the grains: stresses of the order 70–150 Mpa have been measured experimentally (Blendel and Coble, 1982) and stresses of a similar magnitude have been predicted theoretically (Ortiz and Molinari, 1988, Ortiz and Suresh, 1990). According to Evans et al (1977), grains in a state of residual compression are less likely to be fractured by a growing crack and may be left behind as bridging particles. Evans has pointed out that compressive grains may be thought of as regions of increased toughness, and has suggested an expression relating the magnitude of the compressive stress and the grain size to the equivalent toughness of the particles.

Several criteria must be satisfied in order to maximise the toughening due to crack bridging. The elastic modulus of the particles must not exceed that of the matrix material, otherwise the crack tends to be deflected away from the particles. The toughening is also sensitive to the strength of the bond between the particles and matrix. Weakly bonded particles are pulled out in the wake of the crack and increase toughness by frictional energy dissipation (McHugh et al, 1966; Hing and Groves, 1972). Particles firmly bonded to the matrix fracture in the wake of the crack.

A number of calculations have been done to estimate the toughening effect of crack

bridging. Many of these are concerned with frictionally constrained fibres in ceramics (Aveston and Kelly, 1973; Hannant et al, 1983; Marshall and Cox, 1985; Budiansky et al, 1986; Budiansky and Amazigo, 1989; Sigl and Evans, 1989). Other models consider ceramics containing ductile particles (Budiansky, 1986, Budiansky, Amazigo and Evans, 1988). Several studies are devoted to crack bridging in concrete (Hillerborg et al, 1976; Velazco et al, 1980; Wecharatana and Shah, 1982; Ballarini et al, 1984). The essential features of these models are similar: they consider a two–dimensional (plane strain) crack with a bridged zone behind its tip. The effect of this zone is represented by a distribution of pressure $p(\delta)$, acting on the crack flanks. The simplest models assume that p is a linear function of the crack opening displacements δ (Rose, 1987). More complicated expressions have been used to model ductile particles or frictionally constrained fibres. The two–dimensional calculations predict substantial improvements in toughness due to bridging: increases of 10–20 times the matrix toughness have been estimated for a brittle material reinforced by ductile particles, and 2–4 times for a fibre reinforced solid.

There are, however, some shortcomings associated with two–dimensional models of crack bridging. The effect of the crack front bowing between obstacles cannot be taken into account. Separate analyses suggest that crack trapping may considerably influence toughness (Lange, 1970; Evans, 1972; Rose, 1975; Fares, 1990; Gao and Rice, 1990; Bower and Ortiz, 1990). It is also difficult to estimate an appropriate form for the $p - \delta$ relation. Particles properly bonded to the matrix are highly constrained, and so behave elastically even when subjected to loads up to 6 times their yield stress (Ashby et al, 1989). The particles therefore essentially pin discrete points on the faces of the crack. While it is sensible to represent the discrete pinning points as a distribution of pressure if the length of the bridging zone greatly exceeds the particle spacing, this approximation breaks down if there are only a few intact particles behind the crack front.

Until recently, a full three dimensional analysis of crack bridging has been beyond the scope of conventional numerical methods. However, progress in the area of weight function theory in fracture mechanics has provided an invaluable tool for solving problems of this nature. Two different approaches have been proposed. The first is a standard boundary integral formulation, where the crack is represented by a three–dimensional distribution of dislocations. The computing effort required in this procedure may be significantly reduced by using a solution found by Rice (1985) for the interaction of a point dislocation with a crack front as a kernel. This technique was developed by Fares (1990) to solve the problem of a crack bowing out between obstacles.

A second approach is based on work by Rice (1985, 1987) and Gao and Rice (1986,

1987), who developed a linear perturbation scheme for calculating the variation in stress intensity factor due to small changes in crack geometry. This method was used by Gao and Rice (1990) to find first order solutions for the shape of a crack front trapped by an array of tough obstacles. Their analysis was restricted to the situation where the particle toughness exceeds that of the matrix material by a small amount, so that the crack front penetrates the obstacles rather than bypassing them. More recently, Bower and Ortiz (1990) followed a suggestion by Rice (1987) to extend the perturbation method to arbitrarily large changes in crack geometry. They then applied this technique to find the shape of a crack front as it bypasses the array of obstacles. Their results were in good agreement with those of Fares (1990). In this paper, the finite perturbation method is extended to take into account the effects of pinning particles in the wake of the crack, and is used in a three dimensional analysis of crack bridging.

The problem to be solved is illustrated in Fig 2. Consider an unbounded elastic solid containing a straight, semi-infinite crack on the plane $x_3 = 0$, oriented so that its front is parallel to the x_2 axis. The solid is subjected to remote loads, which set up a uniform distribution of mode I stress intensity $K(s) = K^\infty$ along the crack front. Now, assume that there is a doubly periodic distribution of particles, with spacing L in the solid ahead of the crack front. For simplicity, the elastic constants of the particles and matrix material are taken to be identical, but the fracture toughness of the particles K_c^{par} exceeds that of the matrix K_c^{mat}. The particles may be cylindrical, with the axis of each cylinder parallel to the x_3 axis, this would be representative of a fibre-reinforced material. Alternatively, the particles may be spherical, with the centre of the particles on the plane $x_3 = 0$ (a typical configuration in a ceramic reinforced with metallic particles). In either case, the $x_3 = 0$ plane ahead of the crack front contains a distribution of circular regions, radius R, where the toughness exceeds that of the matrix. Initially, we assume that the particles are perfectly bonded to the matrix material. The analysis is subsequently extended to allow particles to be pulled out in the wake of the crack. We now seek to calculate the behaviour of the crack as it propagates through the composite.

Qualitatively, the behaviour of the crack is as follows. When the remote stress reaches a magnitude such that $K^\infty = K_c^{mat}$, the crack begins to propagate through the solid. Eventually, parts of the crack front run into the tough particles. Since $K(s) < K_c^{par}$, these parts arrest. When the remote load is increased by a small amount the remainder of the crack front starts to bow out between the pinning particles, Fig 1. The shape of the bow is determined by the condition that $K(s) = K_c^{mat}$ over the propagating regions, while $K(s) \leq K_c^{par}$ over regions in contact with an obstacle. There are two possible ways in which

the crack can propagate past the row of particles. If K_c^{par} is less than a critical value, to be determined, then the particles are penetrated by the crack front and eventually fracture. The sequence of trapping, penetration and fracture repeats as the crack propagates through the solid. Alternatively, the crack may bow out between the obstacles to such an extent that parts of its front on the far side of the paticle begin to attract one another. Beyond this point, the crack continues to grow unstably under decreasing remote load. Eventually, the crack joins up on itself, leaving behind a row of circular bridging particles. The semi-infinite crack front then continues to propagate until the next row of obstacles is reached, whereupon the process is repeated. Several rows of bridging particles may form in the wake of the crack in this manner. However, the particles cannot remain intact indefinitely, and may fail by one of two mechanisms. If the particles are strongly bonded to the matrix, they fracture in the wake of the crack without appreciable pull-out. Alternatively, if K_c^{par} is large compared to the strength of the bond, the particles remain intact, and are pulled out in the wake of the crack. If the toughness of the interface is low, the pull-out is resisted mainly by friction forces acting between the particle and the matrix, which decrease as the particle is pulled free.

Analysis of this problem involves calculating stress intensity factors for a semi-infinite crack with an arbitrarily shaped front, with its faces pinned over small circular regions. It proves convenient to solve the problem in stages. The solution begins with a straight semi-infinite crack subjected to remote loads. The bridging particles are then added, by finding a distribution of point loads on the crack so as to pin its faces over small circular regions. This part of the analysis is approximate, in that the particle radius is assumed to be much smaller than the spacing. Next, the crack front is perturbed from its straight configuration using the method described in Bower and Ortiz (1990), until the fracture criterion is satisfied on its front. Finally, the crack is marched around a row of obstacles by applying a further succession of first order perturbations. In this way, a complete picture of the behaviour of the crack as it bypasses each row of obstacles can be built up.

2. Theory

2.1 Straight crack perfectly pinned by arrays of particles

Consider the straight, semi-infinite crack shown in Fig. 2 subjected to remote loading, so that a uniform mode I stress intensity factor $K(s) = K^\infty$ is induced on the crack front.

Initially, the crack is free of pinning particles, and the displacement at $\mathbf{x}$ is $\Lambda U(\mathbf{x})$, with

$$U(\mathbf{x}) = 2K^\infty \sqrt{\frac{-x_1}{2\pi}}, \qquad (2.1)$$

$$\Lambda = \frac{(1-\nu)}{\mu}, \qquad (2.2)$$

where ν is Poisson's ratio and μ the shear modulus. Now, a single bridging particle may be introduced in the wake of the crack by finding an appropriate distribution of point loads over the pinned region. First, note that the displacement at $\mathbf{x}$ due to a pair of unit wedging forces acting at $\boldsymbol{\xi}$ is $\Lambda G(\boldsymbol{\xi}, \mathbf{x})$ (Ulfyand, 1965), where

$$G(\boldsymbol{\xi}, \mathbf{x}) = \frac{1}{\pi^2 \rho} \arctan \left\{ 2\sqrt{\frac{x_1 \xi_1}{\rho}} \right\}, \qquad (2.3)$$

$$\rho = \left[(x_1 - \xi_1)^2 + (x_2 - \xi_2)^2 \right]^{1/2}.$$

Distributing wedging forces over a circular domain Ω, radius R, centered at $\mathbf{x}^{(n)}$ on the crack faces then gives rise to the following displacement at $\mathbf{x}$

$$v(\mathbf{x}) = \Lambda U(\mathbf{x}) + \Lambda \int_\Omega G(\boldsymbol{\xi}, \mathbf{x}) p(\boldsymbol{\xi}) d\boldsymbol{\xi}. \qquad (2.4)$$

If the crack faces are completely pinned by the bridging particle, then $v(\mathbf{x}) = 0$ for $\mathbf{x} \in \Omega$, and (2.4) gives an integral equation for the unknown distribution of wedging forces $p(\boldsymbol{\xi})$ on the particle. Note that it is not necessary to enforce complete closure over Ω: any arbitrary relation between v and p could be prescribed. In this way, the analysis may be extended to model debonding between the particle and the matrix, or plastic deformation in the particle. This issue is addressed in section 2.4, but for simplicity we begin by assuming that the particle is perfectly bonded and $v(\mathbf{x}) = 0$.

Equation (2.4) cannot be solved analytically in its present form. However, if the particle radius is much smaller than the distance to the crack front, $G(\boldsymbol{\xi}, \mathbf{x})$ may be simplified as follows. Begin by expressing G in terms of polar co-ordinates centered at $\mathbf{x}^{(n)}$, Fig. 2

$$G(r', \theta', r, \theta) = \frac{1}{\pi^2 \rho} \arctan \left\{ 2\sqrt{\frac{(x_1^{(n)} - r\cos\theta)(x_1^{(n)} - r'\cos\theta')}{\rho}} \right\}, \qquad (2.5)$$

$$\rho = \left[r^2 + r'^2 - 2rr' \cos(\theta - \theta') \right]^{1/2}.$$

Expanding the arctan in (2.5) to first order in $\rho / x_1^{(n)}$, and letting $r/x_1^{(n)}, r'/x_1^{(n)} \to 0$ then leads to the following approximation to G

$$G(\boldsymbol{\xi}, \mathbf{x}) \approx \frac{1}{\pi^2 \rho} \left(\frac{\pi}{2} + \frac{\rho}{2x_1^{(n)}} \right). \qquad (2.6)$$

8

Similarly, we may write $U(\mathbf{x}) \approx U(\mathbf{x}^{(n)})$ to the same order of accuracy. The first term on the right hand side of (2.6) represents the displacement field in a half–space due to point loading. The second term corrects the solution for the presence of undamaged material ahead of the crack front.

For $R << x_1^{(n)}$, the integral equation (2.4) therefore reduces to

$$0 = U(\mathbf{x}^{(n)}) + \frac{1}{\pi^2} \int_\Omega \left(\frac{\pi}{2\rho} + \frac{1}{2x_1^{(n)}} \right) p(\rho, \theta) \, d\rho \, d\theta. \tag{2.7}$$

A similar equation arises in the analysis of a rigid circular punch indenting a half–space, with $p(\boldsymbol{\xi})$ as the unknown pressure between the contacting surfaces, and $\Lambda U(\mathbf{x}^{(n)})$ their normal approach (Ulfyand, 1965). The solution has the form

$$p(\rho) = \frac{P}{4\pi R^2} \left[\sqrt{\frac{R+\rho}{R-\rho}} + \sqrt{\frac{R-\rho}{R+\rho}} \right], \tag{2.8}$$

$$\rho = \left[(x_1^{(n)} - \xi_1)^2 + (x_2^{(n)} - \xi_2)^2 \right], \qquad \boldsymbol{\xi} \in \Omega.$$

where P is the resultant of the pressure distribution. Substituting for $p(\rho)$ in (2.7) and integrating, we obtain an expression which may be solved for P

$$0 = U(\mathbf{x}^{(n)}) + \left(\frac{P}{4R} + \frac{P}{2\pi^2 x_1^{(n)}} \right). \tag{2.9}$$

Here, $P/4R$ represents the displacement under a circular punch indenting a half–space and is independent of the position of the crack. The second term corrects the solution for the constraining effect of the unbroken surface ahead of the crack.

Now, noting that the pressure distribution (2.8) is square root singular at $\rho = R$, the stress intensity on the crack front around the pinning particle may be calculated in the usual way, with the result

$$K^{\mathrm{par}} = -\frac{P}{2R\sqrt{\pi R}}. \tag{2.10}$$

The negative sign in equation (2.10) is a consequence of the sign convention for G, which was chosen so that the positive forces acting on the crack faces tend to open the crack. The pressure on the pinning particles is compressive, so $P < 0$. Equation (2.10) corresponds to the well known solution for the stress intensity on an external circular crack subjected to uniform remote tension.

Finally, the stress intensity factor on the straight crack front may be corrected for the presence of the pinning particle. To first order in $R/x_1^{(n)}$, the pinning particle may be

approximated by a pair of wedging forces, magnitude P, acting on the crack faces. They induce a stress intensity factor $K(s) = PH(s, \mathbf{x}^{(n)})$, where

$$H(s, \mathbf{x}^{(n)}) = \sqrt{\frac{2}{\pi^3}} \cdot \frac{\sqrt{-x_1^{(n)}}}{(s^2 + (x_1^{(n)})^2)}. \tag{2.11}$$

The total stress intensity factor is therefore given by

$$K(s) = K^\infty + PH(s, \mathbf{x}^{(n)}). \tag{2.12}$$

It is straightforward to extend the preceding analysis to allow for an arbitrary number of pinning particles: the configuration shown on Fig. 2 is of particular interest. The crack is now pinned by N parallel rows of circular particles. The spacing between particles in the x_2 direction is L, but otherwise their positions are arbitrary, and may be specified in terms of the co-ordinates $\mathbf{x}^{(n)}$ of a chosen particle on the nth row.

We may write down a closure condition analogous to equation (2.9) for each row of particles. It is only necessary to add the effects of interactions between the particles. To this end, we make use of the additional assumption that the spacing between particles greatly exceeds their radius, so that the displacement at $\mathbf{x}$ due to a particle at $\boldsymbol{\xi}$ may be found by replacing the particle with a pair of wedging forces. This immediately leads to

$$0 = U(\mathbf{x}^{(n)}) + P^{(n)} \left(\frac{1}{4R} + \frac{1}{2\pi^2 x_1^{(n)}} + \sum_{\substack{m=-\infty \\ m \neq 0}}^{\infty} G(\mathbf{x}^{(n)} + mL\mathbf{j}, \mathbf{x}^{(n)}) \right)$$
$$+ \sum_{\substack{k=1 \\ k \neq n}}^{N} P^{(k)} \sum_{m=-\infty}^{\infty} G(\mathbf{x}^{(k)} + mL, \mathbf{x}^{(n)}), \tag{2.13}$$

where $P^{(n)}$ is now the pinning force on a particle in the nth row, and $\mathbf{j}$ is a unit vector in the x_2 direction. It will prove convenient later to simplify this result by defining a new function $\mathbf{G}$ given by

$$\mathbf{G}(\mathbf{x}^{(n)}, \mathbf{x}^{(k)}) = \begin{cases} \dfrac{1}{4R} + \dfrac{1}{2\pi^2 x_1^{(n)}} + \displaystyle\sum_{\substack{m=-\infty \\ m \neq 0}}^{\infty} G(\mathbf{x}^{(n)} + mL\mathbf{j}, \mathbf{x}^{(n)}), & n = k; \\[4mm] \displaystyle\sum_{m=-\infty}^{\infty} G(\mathbf{x}^{(k)} + mL\mathbf{j}, \mathbf{x}^{(n)}), & n \neq k. \end{cases} \tag{2.14}$$

Clearly, the function $\mathbf{G}(\mathbf{x}^{(k)}, \mathbf{x}^{(n)})$ represents the displacement at a particle in the the nth row due to the pinning forces acting on the kth row. Equation (2.13) may now be written

$$0 = U(\mathbf{x}^{(n)}) + \sum_{k=1}^{N} P^{(k)} \mathbf{G}(\mathbf{x}^{(n)}, \mathbf{x}^{(k)}). \tag{2.15}$$

10

giving a set of N linear equations which may be solved for the unknown $P^{(n)}$. The total number of rows of particles N may be found from the condition that the stress intensity factor on the last row must not exceed the particle toughness. From equation (2.10), this gives

$$|P^{(N)}| \leq 2R\sqrt{\pi R}K_c^{\mathrm{par}}. \tag{2.16}$$

Similarly, the expression for the corrected stress intensity factor on the straight crack front (equation (2.12)) becomes

$$K(s) = K^\infty + \sum_{n=1}^{N} P^{(n)} \sum_{m=-\infty}^{+\infty} H(s, \mathbf{x}^{(n)} + mL\mathbf{j}), \tag{2.17}$$

which may be simplified by putting

$$\mathbf{H}(s, \mathbf{x}^{(n)}) = \sum_{m=-\infty}^{+\infty} H(s, \mathbf{x}^{(n)} + mL\mathbf{j}) = \sqrt{\frac{-2x_1}{\pi^3}} \frac{(\sinh 2\pi\gamma)/(2\pi\gamma)}{(L/\pi)^2(\sinh^2 \pi\gamma + \sin^2 \pi\eta)}. \tag{2.18}$$

where $\gamma = -x_1^{(n)}/L$ and $\eta = (s - x_2^{(n)})/L$ to give

$$K(s) = K^\infty + \sum_{n=1}^{N} P^{(n)} \mathbf{H}(s, \mathbf{x}^{(n)}). \tag{2.19}$$

It is now possible to estimate the magnitude of the remote load (paramaterised by K^∞) required to advance the crack through the material. Strictly speaking, it is necessary to enforce the condition $K(s) = K_c^{\mathrm{mat}}$ at all points on the crack front at fracture. However, once the bridging particles have been added to the wake of the crack, the stress intensity factor on its front is no longer uniform. Consequently, it is not possible to satisfy the fracture criterion exactly without changing the shape of the crack front. This issue is addressed in the next section. Nevertheless, it is possible to obtain an accurate estimate of the increase in toughness due to bridging by setting the *average* stress intensity factor along the crack front equal to K_c^{mat}. It is straightforward to show that the mean value of $K(s)$ is:

$$\langle K(s) \rangle = \frac{1}{L} \int_0^L K(s)ds = K^\infty + \sum_{n=1}^{N} \frac{P^{(n)}}{L} \sqrt{\frac{-2}{\pi x_1^{(n)}}} \tag{2.20}$$

whence the toughening ratio is given by

$$\frac{K^\infty}{K_c^{\mathrm{mat}}} \approx \left\{ 1 + \sqrt{\frac{2}{\pi}} \sum_{n=1}^{N} \frac{P^{(n)}}{LK^\infty\sqrt{x_1^{(n)}}} \right\}^{-1} \tag{2.21}$$

11

By way of illustration, it may be shown that for the special case of a *single* row of particles, distance b behind the crack front

$$\frac{P^{(1)}}{LK^\infty} = -\sqrt{\frac{2b}{\pi}} \left\{ \frac{L}{4R} - \frac{L}{2\pi^2 b} + \frac{2F(b/L)}{\pi} \right\}^{-1}, \tag{2.22}$$

$$\frac{K^\infty}{K_c^{mat}} \approx \frac{\pi L/(8R) - L/(4\pi b) + F(b/L)}{\pi L/(8R) - L/(4\pi b) + F(b/L) - 1}, \tag{2.23}$$

$$\frac{K^{par}}{K_c^{mat}} = \frac{L}{2R} \sqrt{\frac{b}{2R}} \frac{1}{\pi L/(8R) - L/(4\pi b) + F(b/L) - 1}, \tag{2.24}$$

where

$$F(x) = \frac{1}{\pi} \sum_{m=1}^\infty \frac{1}{m} \arctan\left(\frac{2x}{m}\right) \tag{2.25}$$

2.2) Extension to wavy cracks

It is evident from the preceding discussion that the crack front will have a wavy profile at fracture. In addition, parts of the crack may bow out between trapping particles. In order to take into account these effects, it is necessary to extend the analysis to cracks with an arbitrarily shaped front; this issue is addressed next.

The following approach will be used. The analysis described in the previous section makes use of three functions: $U(x)$, giving the displacement at x under a uniform remote load; $G(x, \xi)$, which gives the displacement at x due to point loads applied at ξ; and $H(s, x)$, which gives the stress intensity factor at a point s on the crack front due to wedging forces at x. Clearly, if U G and H could be found for an arbitrarily shaped crack, the procedure outlined in section 2.1 could be applied in the same way to add rows of pinning particles. In practice, the functions are known exactly only for circular and semi–infinite cracks. However, it is possible to calculate the *change* in the functions caused by a small perturbation to the geometry of the crack, using the procedure developed by Rice (1985). By applying a succession of such perturbations, G, H and U may then be progressively updated for a crack with an arbitrarily shaped front. The equations involved, cannot be solved analytically, so a numerical procedure is used.

We begin by summarising Rice's equations for the effects of a first–order perturbation in geometry. For details of the derivation of these results, the reader is referred to the work of Rice (1985,1987), Gao and Rice (1986,1987) and Bower and Ortiz (1990). Consider a planar semi–infinite crack with an arbitrarily shaped front, and assume that the functions $G(x, \xi)$, $H(s, \xi)$ and $U(\xi)$ are known for this configuration. In addition, assume that the

12

crack is subjected to remote loading, so that there is an initial mode I stress intensity factor $K(s)$ on the crack front. The magnitude of the load will be parameterised by a remotely applied stress intensity factor K^∞, defined by considering the energy released during an infinitessimal crack advance in the x_1 direction. Given $K(s)$, K^∞ is found to be

$$K^\infty = \sqrt{\frac{1}{L} \int_0^L K^2(x_2)\, dx_2}, \qquad (2.26)$$

where L is one wavelength of the crack front.

It is convenient at this point to introduce another weight function for the crack, defined by

$$D(s,t) = \lim_{\epsilon \to 0} \sqrt{\frac{\pi^3}{?}} \frac{H(s, \mathbf{z}(t) - \epsilon \mathbf{n}(t))}{\sqrt{\epsilon}}, \qquad (2.27)$$

where $\mathbf{z}(t)$ is the position vector of a point t on the crack front C, and $\mathbf{n}(t)$ is the normal to C. Evidently, D represents the stress intensity factors at a point s on the crack front as a pair of square-root singular wedging forces approach the crack front at t. The significance of this weight function is discussed in Bower and Ortiz (1990). For instance, using (2.11), it is easy to show that for a straight crack

$$D(s,t) = \frac{1}{(t-s)^2}. \qquad (2.28)$$

Now, imagine allowing the crack to advance by a small amount $\delta a(s)\mathbf{n}(s)$. The following equations may then be shown to hold, accurate to first order in $\delta a(s)$:

$$\delta U(\mathbf{x}) = \frac{\delta K^\infty}{K^\infty} U(\mathbf{x}) + \frac{1}{2} \int_C K(s) H(s,\mathbf{x}) \delta a(s)\, ds, \qquad (2.29)$$

$$\delta G(\mathbf{x},\boldsymbol{\xi}) = \frac{1}{2} \int_C H(s,\boldsymbol{\xi}) H(s,\mathbf{x}) \delta a(s)\, ds, \qquad (2.30)$$

$$\delta K(s) = \frac{\delta K^\infty}{K^\infty} K_0(s) + \frac{1}{2\pi} \int_C K(t) D(t,s)[\delta a(t) - \mathbf{n}(s) \cdot \mathbf{n}(t) \delta a(s)]\, dt, \qquad (2.31)$$

$$\delta H(s,\mathbf{x}) = \frac{1}{2\pi} \int_C H(\lambda,\mathbf{x}) D(s,\lambda) \left\{ \delta a(\lambda) - \right.$$
$$\left. \frac{[\mathbf{x} - \mathbf{z}(\lambda)] \cdot [\mathbf{x} - \mathbf{z}(s)]}{[\mathbf{x} - \mathbf{z}(s)] \cdot [\mathbf{x} - \mathbf{z}(s)]} \mathbf{n}(\lambda) \cdot \mathbf{n}(s) \delta a(s) \right\} d\lambda$$
$$- \frac{\delta a(s)}{2\pi} \int_C H(\lambda,\mathbf{x}) D(s,\lambda) \frac{[(\mathbf{x} - \mathbf{z}(\lambda)) \times (\mathbf{x} - \mathbf{z}(s))] \cdot \mathbf{k}}{[\mathbf{x} - \mathbf{z}(s)] \cdot [\mathbf{x} - \mathbf{z}(s)]} [\mathbf{n}(\lambda) \times \mathbf{n}(s)] \cdot \mathbf{k} d\lambda$$
$$+ H(s,\mathbf{x}) \frac{3\delta a(s)}{2} \frac{[\mathbf{x} - \mathbf{z}(s)] \cdot \mathbf{n}(s)}{[\mathbf{x} - \mathbf{z}(s)] \cdot [\mathbf{x} - \mathbf{z}(s)]}, \qquad (2.32)$$

$$\delta D(s,t) = \frac{1}{2\pi} \int_C D(\lambda,t) D(s,\lambda) \left\{ \delta a(\lambda) - \right.$$

$$\frac{[\mathbf{z}(s) - \mathbf{z}(t)] \cdot [\mathbf{z}(\lambda) - \mathbf{z}(t)]}{[\mathbf{z}(t) - \mathbf{z}(s)] \cdot [\mathbf{z}(t) - \mathbf{z}(s)]} \mathbf{n}(\lambda) \cdot \mathbf{n}(s) \delta a(s)$$

$$- \frac{[\mathbf{z}(t) - \mathbf{z}(s)] \cdot [\mathbf{z}(\lambda) - \mathbf{z}(s)]}{[\mathbf{z}(t) - \mathbf{z}(s)] \cdot [\mathbf{z}(t) - \mathbf{z}(s)]} \mathbf{n}(\lambda) \cdot \mathbf{n}(s) \delta a(t) \bigg\} \, d\lambda$$

$$- \frac{\delta a(s)}{2\pi} \int_C D(\lambda,t) D(s,\lambda) \frac{[\mathbf{z}(\lambda) - \mathbf{z}(t)] \times [\mathbf{z}(s) - \mathbf{z}(t)] \cdot \mathbf{k}}{[\mathbf{z}(t) - \mathbf{z}(s)] \cdot [\mathbf{z}(t) - \mathbf{z}(s)]} \mathbf{n}(\lambda) \times \mathbf{n}(s) \cdot \mathbf{k} d\lambda$$

$$- \frac{\delta a(t)}{2\pi} \int_C D(\lambda,t) D(s,\lambda) \frac{[\mathbf{z}(\lambda) - \mathbf{z}(s)] \times [\mathbf{z}(t) - \mathbf{z}(s)] \cdot \mathbf{k}}{[\mathbf{z}(s) - \mathbf{z}(t)] \cdot [\mathbf{z}(s) - \mathbf{z}(t)]} \mathbf{n}(\lambda) \times \mathbf{n}(t) \cdot \mathbf{k} d\lambda$$

$$- 2D(s,t) \frac{[\delta a(t)\mathbf{n}(t) - \delta a(s)\mathbf{n}(s)] \cdot [\mathbf{z}(t) - \mathbf{z}(s)]}{[\mathbf{z}(t) - \mathbf{z}(s)] \cdot [\mathbf{z}(t) - \mathbf{z}(s)]}. \tag{2.33}$$

Here, $\int_C$ denotes integration around the crack front; $(\times)$ and $(\cdot)$ are vector and scalar products. In equations (2.29) and (2.31), the terms involving $\delta K^\infty / K^\infty$ represent changes due to an increment in the remote load; the remaining terms are changes due to the perturbation in crack geometry. Equations (2.32) and (2.33), which are modified forms of Rice's results, are derived in Appendix A. The remaining equations may be found in Rice (1985, 1987).

These results are the basis of an incremental method for calculating stress intensity factors and weight functions for any arbitrarily shaped crack. For example, stress intensity factors may be calculated by repeatedly applying equations (2.31) and (2.33). The analysis begins with a convenient reference geometry for which stress intensities and influence functions are known in closed form, such as a circular or semi–infinite crack. Equation (2.31) is then used to calculate the change in stress intensity caused by a small change in the shape of the crack. The problem may be posed in one of two ways: we may either find changes due to a prescribed crack advance; or alternatively, we may calculate the displacement of the crack front consistent with a given crack growth criterion, such as $K(s) = K_c(\mathbf{z}(s))$. In the latter case, (2.31) is a singular integral equation to be solved for $\delta a(s)$. Once the new shape of the crack has been found, equation (2.33) is used to calculate a new weight function D for the perturbed geometry. Similarly, the crack face displacements U, and the weight functions G and H may be updated using equations (2.29), (2.30) and (2.32). This process may be repeated ad infinitum: by successively updating the crack geometry and influence functions, we may calculate the effect of an arbitrarily large displacement of the crack front. In actual calculations, the governing integral equations are discretised using standard numerical techniques. A method of solution has been described by Bower and Ortiz (1990), and is summarised briefly in Section 2.5. Since the appropriate equations are accurate to first order in $\delta a(s)$, the numerical solution may be expected to converge as the amplitude of each successive perturbation and the mesh size are progressively reduced.

For the particular case of a periodic perturbation of a semi–infinite crack, equations (2.29) to (2.31) may be simplified by reducing the integrals to one wavelength of the crack front. In addition, it is possible to derive incremental expressions for the summed weight functions $\mathbf{G}$ and $\mathbf{H}$ defined in equations (2.14) and (2.18). The derivations are somewhat laborious, and are given in appendix B. Here, we merely summarise the results. Consider allowing the front of a semi–infinite crack to advance by a small amount $\delta a(s)$, which is periodic in the x_2 direction so that

$$\delta a(s + mc) = \delta a(s), \tag{2.34}$$

where c is the arc length along one wavelength ($c = L$ for a straight crack), and m is any integer. It then follows that

$$\delta U(\mathbf{x}) = \frac{\delta K^\infty}{K^\infty} U(\mathbf{x}) + \frac{1}{2} \int_{-c/2}^{c/2} K_0(s) \mathbf{H}(s, \mathbf{x}) \delta a(s) \, ds, \tag{2.35}$$

$$\delta \mathbf{G}(\mathbf{x}^{(n)}, \mathbf{x}^{(k)}) = \frac{1}{2} \int_{-c/2}^{c/2} \mathbf{H}(s, \mathbf{x}^{(n)}) \mathbf{H}(s, \mathbf{x}^{(k)}) \delta a(s) \, ds, \tag{2.36}$$

$$\delta K(s) = \frac{\delta K^\infty}{K^\infty} K(s) + \frac{1}{2\pi} \int_{-c/2}^{c/2} K(\lambda) \mathbf{D}(\lambda, s) [\delta a(\lambda) - \delta a(s) \mathbf{n}(\lambda) \cdot \mathbf{n}(s)] \, d\lambda, \tag{2.37}$$

$$\delta \mathbf{H}(s, \mathbf{x}) = \frac{1}{2\pi} \int_{-c/2}^{c/2} \mathbf{H}(\lambda, \mathbf{x}) \mathbf{D}(\lambda, s) [\delta a(\lambda) - \delta a(s) \mathbf{n}(\lambda) \cdot \mathbf{n}(s)] \, d\lambda$$
$$+ \delta a(s) \mathbf{\Psi}(s, \mathbf{x}), \tag{2.38}$$

where:

$$\mathbf{D}(s, t) = \sum_{m=-\infty}^{+\infty} D(s + mc, t) \tag{2.39}$$

$$\mathbf{\Psi}(s, \mathbf{x}) = \frac{1}{2\pi} \int_{-c/2}^{c/2} \sum_{n=-\infty}^{+\infty} \sum_{m=-\infty}^{+\infty} H(\lambda, \mathbf{x} + (m - n)L\mathbf{j}) D(\lambda + nc, s)$$

$$\left\{ \frac{[\mathbf{z}(s) - \mathbf{z}(\lambda) + -nL\mathbf{j}] \cdot [\mathbf{x} - \mathbf{z}(s) + mL\mathbf{j}]}{[\mathbf{x} - \mathbf{z}(s) + mL\mathbf{j}] \cdot [\mathbf{x} - \mathbf{z}(s) + mL\mathbf{j}]} [\mathbf{n}(\lambda) \cdot \mathbf{n}(s)] \right.$$

$$\left. - \frac{[\mathbf{x} - \mathbf{z}(\lambda) + (m - n)L\mathbf{j}] \times [\mathbf{x} - \mathbf{z}(s) + mL\mathbf{j}] \cdot \mathbf{k}}{[\mathbf{x} - \mathbf{z}(s) + mL\mathbf{j}] \cdot [\mathbf{x} - \mathbf{z}(s) + mL\mathbf{j}]} [\mathbf{n}(\lambda) \times \mathbf{n}(s)] \cdot \mathbf{k} \right\} d\lambda \tag{2.40}$$

$$+ \frac{3}{2} \sum_{m=-\infty}^{+\infty} H(s, \mathbf{x} + mL\mathbf{j}) \frac{[\mathbf{x} - \mathbf{z}(s) + mL\mathbf{j}] \cdot \mathbf{n}(s)}{[\mathbf{x} - \mathbf{z}(s) + mL\mathbf{j}] \cdot [\mathbf{x} - \mathbf{z}(s) + mL\mathbf{j}]}$$

The updated influence functions $\mathbf{G}$ and $\mathbf{H}$ may be used to add pinning particles to the wake of the crack as outlined in section 2.1 For a semi–infinite crack pinned by N rows

15

of parallel circular particles, the pinning force on each row of obstacles is calculated using the closure condition (2.15). Here, we have assumed without proof that for $R/L << 1$, the distribution of pressure on each pinned region is unchanged by modifying the crack front, and may still be characterised by its resultant P. This is justified in Appendix B. The stress intensity factors on the crack front are then found from (2.19)

In general, once pinning particles have been added to the wake of the crack, it is necessary to modify the crack geometry in order to satisfy the fracture criterion at all points on the crack front. For example, it was shown in section 2.1 that when pinning particles are added to a straight crack, the condition $K(s) = K_c^{\mathbf{mat}}$ can only be met by perturbing the crack front. This issue is addressed next.

The problem may be stated as follows. We wish to find a crack advance $\delta a(s)$ that changes the stress intensities on the crack front by a known amount $\delta K(s)$, such that $K(s) + \delta K(s) = K_c(\mathbf{z}(s))$. At the same time, we wish to satisfy the closure condition on each particle for the perturbed geometry. To this end, we write down expressions similar to (2.15) and (2.19) for the perturbed crack:

$$0 = U(\mathbf{x}^{(n)}) + \delta U(\mathbf{x}^{(n)}) + \sum_{k=1}^{N} \left(P^{(k)} + \delta P^{(k)} \right) \left(\mathbf{G}(\mathbf{x}^{(k)}, \mathbf{x}^{(n)}) + \delta \mathbf{G}(\mathbf{x}^{(k)}, \mathbf{x}^{(n)}) \right), \quad (2.41)$$

$$K(s) + \delta K(s) = K_0(s) + \delta K_0(s) + \sum_{k=1}^{N} \left(P^{(k)} + \delta P^{(k)} \right) \left(\mathbf{H}(s, \mathbf{x}^{(n)}) + \delta \mathbf{H}(s, \mathbf{x}^{(n)}) \right) \quad (2.42)$$

where $\delta P^{(k)}$ is the change in pinning force on the kth row of particles. Neglecting second order terms, and using (2.15) and (2.19), these results may be simplified to

$$0 = \delta U(\mathbf{x}^{(n)}) + \sum_{k=1}^{N} \left(\delta P^{(k)} \mathbf{G}(\mathbf{x}^{(n)}, \mathbf{x}^{(k)}) + P^{(k)} \delta \mathbf{G}(\mathbf{x}^{(n)}, \mathbf{x}^{(k)}) \right), \quad (2.43)$$

$$\delta K(s) = \delta K_0(s) + \sum_{k=1}^{N} \left(\delta P^{(k)} \mathbf{H}(s, \mathbf{x}^{(n)}) + P^{(k)} \delta \mathbf{H}(s, \mathbf{x}^{(n)}) \right). \quad (2.44)$$

Finally, substituting (2.35) to (2.38) into (2.43) and (2.44), and eliminating $K_0(s)$ and $U(\mathbf{x})$ using (2.15) and (2.19), we find that

$$0 = \frac{1}{2} \int_{-c/2}^{c/2} K(\lambda) \mathbf{H}(\lambda, \mathbf{x}^{(n)}) \delta a(\lambda) \, d\lambda + \sum_{k=1}^{N} \left(\delta P^{(k)} - \frac{\delta K^\infty}{K^\infty} P^{(k)} \right) \mathbf{G}(\mathbf{x}^{(n)}, \mathbf{x}^{(k)}), \quad (2.45)$$

$$\delta K(s) = \frac{1}{2\pi} \int_{-c/2}^{c/2} K(\lambda) \mathbf{D}(\lambda, s) [\delta a(\lambda) - \mathbf{n}(\lambda) \cdot \mathbf{n}(s) \delta a(s)] \, d\lambda + \frac{\delta K^\infty}{K^\infty} K(s)$$
$$+ \delta a(s) \sum_{k=1}^{N} P^{(k)} \mathbf{\Psi}(s, \mathbf{x}^{(k)}) + \sum_{k=1}^{N} \left(\delta P^{(k)} - \frac{\delta K^\infty}{K^\infty} P^{(k)} \right) \mathbf{H}(s, \mathbf{x}^{(k)}). \quad (2.46)$$

16

Here, $K(s)$ represents the stress intensity factor on the *pinned* crack: all variables relating to the unpinned crack have been eliminated. Given an increment in stress intensity $\delta K(s)$, (2.45) and (2.46) form a set of $N + 1$ coupled singular integral equations to be solved for $\delta a(s)$ and $\delta P^{(k)}$. Once the new shape of the crack has been found, equations (2.32), (2.33), (2.36) and (2.38) may be used to calculate updated influence functions for the perturbed geometry.

2.3) Application to crack growth through toughened solid

The procedure outlined in the previous section may now be applied to solve the specific problem of a semi–infinite crack propagating through a material containing tough second phase particles. Consider the configuration shown in Fig. 2. A particulate toughened solid contains a straight, semi–infinite crack: initially, the crack faces are free of pinning particles, and we will assume that the crack front is just short of one row of obstacles. Now, imagine applying a steadily increasing remote load to the body. When the load reaches a magnitude $K^\infty = K_c^{\mathrm{mat}}$, the crack starts to propagate around the particle. Parts of the crack front which touch the particle are assumed to arrest, so that $\delta a(s) = 0$ at these points. The crack advance over the remainder of the crack front is determined by the condition that $K(s) = K_c^{\mathrm{mat}}$: this may be satisfied by solving equation (2.37) with $\delta K(s) = 0$. If there are no pinning particles on the crack faces, we obtain the following conditions on the crack advance

$$\delta a(s) = 0 \qquad \text{Crack trapped,} \qquad (2.47)$$

$$0 = \frac{\delta K^\infty}{K^\infty} K(s)$$

$$+ \frac{1}{2\pi} \int_{-c/2}^{c/2} K(\lambda) \mathbf{D}(\lambda, s)[\delta a(\lambda) - \mathbf{n}(\lambda) \cdot \mathbf{n}(s)\delta a(s)] \, d\lambda \qquad \text{Crack propagating. (2.48)}$$

In principle, given an increment in remote load δK^∞, (2.47) and (2.48) may be solved for $\delta a(s)$. However, this may be an ill–conditioned problem, since a very small change in load may cause a large crack advance, particularly when the peak load is approached. In practice, it is preferable to leave the increment in load as an unknown, and enforce an additional constraint on the crack advance. Here, we have chosen to constrain the maximum crack front displacement. The numerical procedure used to solve the singular integral equation (2.48) is described in Bower and Ortiz (1990), and is summarised briefly in the next section.

Once $\delta a(s)$ has been determined over the propagating regions of the crack, $\delta K(s)$ on the arrested parts may be found using (2.37), and the weight function D is updated

using (2.33). In addition, the crack face displacements $U(\mathbf{x})$, and the influence functions $\mathbf{G}(\mathbf{x}, \xi)$ and $H(\mathbf{x}, s)$ are updated at chosen points to allow pinning particles to be added to the crack at a later stage. This procedure is repeated to march the crack front around the first row of obstacles. The behaviour of the crack as it bypasses a row of particles is shown in Fig. 4. As the crack front bows between the inclusions, it eventually reaches a configuration where parts of the crack begin to attract one another. At this point, the applied load reaches a maximum, and the crack subsequently propagates under decreasing remote load. Eventually, the crack joins up on itself on the far side of the obstacle, leaving behind a bridging particle.

It is not possible to analyse the coalescence of the crack using the finite perturbation method. The perturbation procedure only gives accurate results if the change in weight function δD is small compared to D during each step. Equation (2.33) shows that δD varies as $([\mathbf{z}(s) - \mathbf{z}(t)] \cdot [\mathbf{z}(s) - \mathbf{z}(t)])^{-1}$, where $\mathbf{z}(s)$ and $\mathbf{z}(t)$ are the position vectors of points t and s on the crack front. If the crack is about to join up on itself, $\mathbf{z}(s) \to \mathbf{z}(t)$ at the points of coalescence. Consequently, in order for δD to be small, $\delta a(\lambda)$ must become vanishingly small at these points, and an infinite number of time steps are required for the crack to join up. In addition, $D(s, t)$ becomes badly behaved at the point of coalescence, so an extremely fine crack front mesh is required to get accurate numerical results, making the perturbation method prohibitively expensive.

These difficulties may be avoided by using the method outlined in the section 2.1 to add pinning particles to the wake of the crack. We therefore ignore the details of the coalescence, and consider the crack at a slightly later stage. For example, we may resume the analysis at the point when the crack front just short of the second row of obstacles, with a single row of bridging particles in its wake. A crack configuration must now be found that satisfies the appropriate displacement boundary conditions on each pinning particle, and the fracture criterion $K(s) = K_c^{\mathrm{mat}}$ on the crack front. This may be reached in three stages:

(i) Starting with a straight crack in the required position under unit remote load, equation (2.15) is solved to find the magnitude of the pinning force on each particle;

(ii) The magnitude of the remote load K^∞ is adjusted so that the fracture criterion $K(s) = K_c^{\mathrm{mat}}$ at some arbitrary point (say $s = \pm c/2$).

(iii) Finally, the crack front is allowed to advance until the fracture criterion is satisfied at all points its front. To do this, we set $\delta K(s) = K(s) - K_c^{\mathrm{mat}}$ in (2.46), and solve the coupled equations (2.45) and (2.46) for $\delta a(s)$, subject to $\delta K^\infty = 0$. If the necessary $\delta K(s)$ is

large, several small perturbations may be applied to reach the correct configuration.

This procedure may be applied to add pinning particles to the crack at any stage as it bows out between a row of trapping obstacles. A complete picture may then be built up as the crack propagates around several successive rows of obstacles. This approach significantly reduces the computing effort involved in the analysis, since any arbitrary number of rows of obstacles may be added without having to solve for all intermediate configurations of the crack. The actual number of rows of obstacles left intact in the wake of the crack is determined by the particle toughness. Particles are added until the stress intensity factor on the particles furthest from the crack front (calculated using equation (2.10)) exceeds K_c^{par}.

2.4) Frictional crack bridging

In the preceding sections, it was assumed that the particles remain perfectly bonded to the matrix material, and fail by fracture in the wake of the crack. If the interface between particles and matrix is weak, it may fail before the particles fracture. The particles then remain intact and are pulled out in the wake of the crack. The pull–out is resisted by friction forces acting between the particles and matrix, which decrease as the particle is pulled free. The energy dissipated as long grains are pulled out in the wake of a crack is believed to be an important toughening mechanism in monolithic ceramics (Vekinis et al, 1990). In this section, the analysis of a pinned crack is extended to account approximately for frictional pull–out.

The separation of an individual grain from the surrounding material is idealised using the simple model illustrated in Fig. 3. The grain is taken to be cylindrical, radius R and height δ_{crit}. We assume that the particle is pinched into the matrix by thermal stresses, so that a local compressive stress σ_r acts perpendicular to the interface. The force required to pull the grain free by a distance δ is given by

$$P = P_0(1 - \frac{\delta}{\delta_{\text{crit}}}).$$

(2.49)

Here, P_0 is the maximum pinning force on the grain, given by

$$P_0 = \pi f \sigma_r R \delta_{\text{crit}},$$

(2.50)

where f is the coefficient of friction. We note in passing that it is possible to enforce any non–linear relation between crack opening and pinning force. For example, the analysis

19

could be extended to model plastic deformation in the particles. However, this is not pursued here.

Suppose that the matrix contains a regular distribution of similar grains, spacing L. For simplicity, assume that the grains are all aligned, with axes parallel to the x_3 direction. Now, consider the behaviour of a semi–infinite crack in the $x_3 = 0$ plane as it propagates through the solid. The particles trap the front of the crack as before, which bows out between them. We assume that the particles are sufficiently tough never to be penetrated by the crack, so that they are left behind in its wake. The particles remain perfectly pinned until the pinning force exceeds P_0, at which point they start to be separated from the matrix. During pull–out, the pinning force P is related to the crack opening displacement δ by equation (2.49). When $\delta > \delta_{\text{crit}}$, the particle is completely free from the matrix and $P = 0$.

It is straightforward to incorporate this force–crack opening displacement relation into the model of a bridged crack. By relaxing the constraint that $v(\mathbf{x}) = 0$ in equation (2.4), the separation of the crack faces is related to the pinning force by

$$\delta(\mathbf{x}^{(n)}) = 2\Lambda U(\mathbf{x}^{(n)}) + 2\Lambda \sum_{k=1}^{N} P^{(k)} \mathbf{G}(\mathbf{x}^{(n)}, \mathbf{x}^{(k)}). \tag{2.51}$$

Here $\delta(\mathbf{x}^{(n)})$ is the crack opening displacement at the nth row of particles, $\Lambda U(\mathbf{x}^{(n)})$ is the displacement at the same point for the unpinned crack, and $\Lambda \mathbf{G}(\mathbf{x}^{(n)}, \mathbf{x}^{(k)})$ represents the displacent at $\mathbf{x}^{(n)}$ due to the pinning forces on the kth row of particles. For a straight crack, U and $\mathbf{G}$ are given by equations (2.1), (2.3) and (2.14); for a wavy crack they may be found using the perturbation procedure outlined in the previous section. For particles perfectly pinned to the matrix, $\delta(\mathbf{x}^{(n)}) = 0$. For debonding particles, $\delta(\mathbf{x}^{(n)})$ may be found by eliminating $P^{(n)}$ between (2.49) and (2.51). If particles at $\mathbf{x}^{(1)}, \mathbf{x}^{(2)}, \ldots \mathbf{x}^{(N)}$ remain perfectly pinned, while particles at $\mathbf{x}^{(N+1)}, \mathbf{x}^{(N+2)}, \ldots \mathbf{x}^{(M)}$ are debonding, we obtain the following expressions for $P^{(n)}$ and $\delta^{(n)}$

$$-U(\mathbf{x}^{(n)}) = \sum_{k=1}^{M} P^{(k)} \mathbf{G}(\mathbf{x}^{(k)}, \mathbf{x}^{(n)}) \qquad\qquad 1 \le n \le N, \tag{2.52}$$

$$2\Lambda U(\mathbf{x}^{(n)}) - 2\Lambda P_0 \sum_{k=N+1}^{M} \mathbf{G}(\mathbf{x}^{(k)}, \mathbf{x}^{(n)}) = \delta(\mathbf{x}^{(n)}) - \frac{2\Lambda P_0}{\delta_{\text{crit}}} \sum_{k=N+1}^{M} \delta(\mathbf{x}^{(k)}) \mathbf{G}(\mathbf{x}^{(k)}, \mathbf{x}^{(n)})$$

$$- 2\Lambda \sum_{k=1}^{N} P^{(k)} \mathbf{G}(\mathbf{x}^{(k)}, \mathbf{x}^{(n)}) \qquad N < n \le M. \tag{2.53}$$

Equations (2.52) and (2.53) may be solved for the unknown $P^{(k)}$ over the perfectly pinned grains, and $\delta(\mathbf{x}^{(k)})$ at debonding particles. $P^{(k)}$ on debonding particles is then deduced

20

using (2.51). Finally, the stress intensity factor on the semi–infinite crack front is calculated using (2.19).

Although equations (2.52) and (2.53) are linear, the number of perfecly pinned particles N is not known a priori, and must be determined using an iterative procedure. The following technique is used here. Initially, we assume that all particles are perfecly pinned, and solve (2.52) for $P^{(k)}$. The condition that $P^{(k)} < P_0$ is then checked: any grains where this criterion is violated are allowed to debond. A new distribution of P and δ is then calculated, and this procedure is repeated until convergence occurs. Problems involving frictional behaviour are load–history dependent. The solution calculated here implicitly assumes that the crack is subjected to a monotonically increasing load, so that the force on each pinning particle never reverses sign.

For a straight crack, the influence functions $\mathbf{G}$ and $\mathbf{H}$ are known in closed form. For a wavy crack, they may be calculated using the perturbation procedure outlined in section 2.4. However, it is found that in some cases over 500 rows of debonding grains may be left in the wake of the crack: a prohibitive amount of computing time is required to update the influence functions for this number of rows. We have avoided this difficulty by updating $\mathbf{G}$ and $\mathbf{H}$ explicitly for the 10 rows of particles closest to the crack front, and calculating the remainder approximately. The function $\mathbf{G}(\mathbf{x}^{(n)}, \mathbf{x}^{(k)})$ is estimated by replacing the wavy crack front with an equivalent straight crack. The equivalent crack is chosen by matching the average distance between the row of particles and the crack front.

Estimating $\mathbf{H}$ is less straightforward. However, inspection of equation (2.38) shows that if $\mathbf{x} - \mathbf{z}(s) >> \delta a(s)$, the incremental expression for $\mathbf{H}$ may be approximated by

$$\delta\mathbf{H}(s,\mathbf{x}) = \frac{1}{2\pi} \int_{-c/2}^{c/2} \mathbf{H}(\lambda,\mathbf{x}) \mathbf{D}(\lambda,s)[\delta a(\lambda) - \delta a(s)\mathbf{n}(\lambda)\cdot\mathbf{n}(s)] \, d\lambda. \qquad (2.54)$$

Comparison with (2.37) shows that this is equivalent to the expression for $\delta K(s)$, with $K(\lambda) = \mathbf{H}(\lambda,\mathbf{x})$ and $\delta K^\infty = 0$. Let $\mathbf{H}_0(\lambda,\mathbf{x})$ be the magnitude of $\mathbf{H}$ for a straight crack, as defined in (2.18). Noting that $\mathbf{H}_0(\lambda,\mathbf{x})$ is almost independent of λ, and that $K(\lambda)$ is constant, we conclude by induction that if $K(\lambda)$ is known for the wavy crack under a remote load K^∞, $\mathbf{H}$ may be deduced from

$$\mathbf{H}(\lambda,\mathbf{x}) \approx \mathbf{H}_0(\lambda,\mathbf{x})\frac{K(\lambda)}{K^\infty}. \qquad (2.55)$$

Essentially, (2.55) states that the stress intensities induced by a row of point loads applied a long way from the front of a wavy crack may be estimated by replacing the point loads by an equivalent uniform remote stress. The uniform stress is chosen to induce the same

21

stress intensity factor on a straight crack as the point loads. The same result is obtained by matching energy release rates for the two cases. The accuracy of the estimates of G and H has been tested by comparing the approximate values with the exact results calculated using the finite perturbation method. For the tenth row of particles behind the crack front, the error in the approximate solution is less than 1%. Any arbitrary number of debonding particles may thus be added to the wake of the crack.

2.5) Numerical Implementation

The numerical procedure used to add pinning particles to the crack is straightforward, and merely involves solving a set of linear equations. However, special procedures are required to solve the system of singular integral equations that arises during the perturbation of the crack geometry. The numerical technique used to discretise the integral equations follows closely the procedure given in Bower and Ortiz (1990), and will only be briefly summarised here. One wavelength of the crack front is divided into m elements, with three nodes s_{2k-2}, s_{2k-1} and s_{2k} on the kth element. In addition, $2m - 1$ collocation points such that $s_j < t_j < s_{j+1}$ are defined. The crack advance is then approximated using Hermitian interpolation between values of $\delta a(s_{2k})$ and $d\delta a(s_{2k})/ds$ for $k = 1, 2 \ldots m$. The variation of stress intensity factor over each element is approximated by means of a Lagrangian interpolation between nodal values; similarly, to approximate the weight functions H, D, $\mathbf{H}$ and $\mathbf{D}$ we write:

$$H(s + kc, \mathbf{x}^{(n)}) = \frac{h(s + kc, \mathbf{x}^{(n)})}{[\mathbf{z}(s) - \mathbf{x}^{(n)} + kL\mathbf{j}] \cdot [\mathbf{z}(s) - \mathbf{x}^{(n)} + kL\mathbf{j}]}, \tag{2.56}$$

$$D(s + kc, t) = \frac{d(s + mc, t)}{[\mathbf{z}(s) - \mathbf{z}(t) + kL\mathbf{j}] \cdot [\mathbf{z}(s) - \mathbf{z}(t) + kL\mathbf{j}]}, \tag{2.57}$$

$$\mathbf{H}(s, \mathbf{x}^{(n)}) = \frac{\mathbf{h}(s, \mathbf{x}^{(n)})(\sinh 2\pi\theta)/(2\pi\theta)}{(L/\pi)^2(\sin^2 \pi\zeta + \sinh^2 \pi\theta)}, \tag{2.58}$$

$$\mathbf{D}(s, t) = \frac{\mathbf{d}(s, t)(\sinh 2\pi\gamma)/(2\pi\gamma)}{(L/\pi)^2(\sin^2 \pi\eta + \sinh^2 \pi\gamma)}, \tag{2.59}$$

$$\theta = (x_1 - z_1(s))/L; \qquad \zeta = (x_2 - z_2(s))/L$$

$$\gamma = (z_1(s) - z_1(t))/L; \qquad \eta = (z_2(s) - z_2(t))/L$$

and use three point Lagrangian interpolation between nodal values to approximate the functions h, d, $\mathbf{h}$ and $\mathbf{d}$. The functions $h(s + kc, \mathbf{x})$ and $d(s + kc, t)$ need to be stored (and updated) over a number of wavelengths of the crack front, $k = -M, -M + 1 \ldots M - 1, M$, as discussed in Bower and Ortiz (1990). In addition, it is convenient to define two more

22

functions $h_\infty(s, \mathbf{x})$ and $d_\infty(s, t)$, such that

$$h_\infty(s, \mathbf{x}) = \lim_{k \to \infty} h(s \pm kc, \mathbf{x}), \tag{2.60}$$

$$d_\infty(s, t) = \lim_{k \to \infty} d(s \pm kc, t). \tag{2.61}$$

The infinite series in equations (2.18), (2.39) and (2.40) are then evaluated by splitting each series into a periodic and a non–periodic part. The periodic part may be summed explicitly, and the remaining series is summed numerically by truncating it at a finite number of terms. For example, to evaluate the series in (2.39), we write:

$$\frac{\mathbf{d}(s,t)(\sinh 2\pi\gamma)/(2\pi\gamma)}{(L/\pi)^2(\sin^2 \pi\eta + \sinh^2 \pi\gamma)} = \sum_{k=-\infty}^{+\infty} \frac{d(s + kc, t)}{[x_1(s) - x_1(t)]^2 + [x_2(s) - x_2(t) + kL]^2}$$

$$= \sum_{k=-\infty}^{+\infty} \frac{d_\infty(s,t)}{[x_1(s) - x_1(t)]^2 + [x_2(s) - x_2(t) + kL]^2} + \sum_{k=-\infty}^{+\infty} \frac{d(s + kc, t) - d_\infty(s,t)}{[x_1(s) - x_1(t)]^2 + [x_2(s) - x_2(t) + kL]^2}$$

$$\approx \frac{d_\infty(s,t)(\sinh 2\pi\gamma)/(2\pi\gamma)}{(L/\pi)^2(\sin^2 \pi\eta + \sinh^2 \pi\gamma)} + \sum_{k=-M}^{+M} \frac{d(s + kc, t) - d_\infty(s,t)}{[x_1(s) - x_1(t)]^2 + [x_2(s) - x_2(t) + kL]^2}. \tag{2.62}$$

The choice of a suitable value for M is discussed in Bower and Ortiz (1990): normally, $M = 2$ is sufficient. The series in (2.18) and (2.40) may be evaluated in a similar way, but for reasons of space will not be written out in full here.

To solve the integral equations (2.45) and (2.46), the integrands are expressed in terms of nodal values of δa, K, $\mathbf{H}$ and $\mathbf{D}$ by means of the adopted interpolation functions. As a result, the integrals may be evaluated explicitly, and the equations may be written in the linear form

$$0 = \sum_{i=0}^{m} W_i(\mathbf{x}^{(n)})\delta a(s_{2i}) + \hat{W}_i(\mathbf{x}^{(n)})\delta a'(s_{2i})$$

$$+ \sum_{k=1}^{N} \left(\delta P^{(k)} - \frac{\delta K^\infty}{K^\infty} P^{(k)} \right) \mathbf{G}(\mathbf{x}^{(n)}, \mathbf{x}^{(k)}), \tag{2.63}$$

$$\delta K(t_j) = \frac{\delta K^\infty}{K^\infty} K(t_j) + \sum_{i=0}^{m} V_i(t_j)\delta a(s_{2i}) + \hat{V}_i(t_j)\delta a'(s_{2i})$$

$$+ \sum_{k=1}^{N} \left(\delta P^{(k)} - \frac{\delta K^\infty}{K^\infty} P^{(k)} \right) \mathbf{H}(\mathbf{x}^{(n)}, \mathbf{x}^{(k)}), \tag{2.64}$$

where $W_i(\mathbf{x})$, $\hat{W}_i(\mathbf{x})$, $V_i(t)$ and $\hat{V}_i(t)$ are integration weights depending on the current crack configuration. The procedure used to calculate these functions is given in Bower and Ortiz (1990). Equations (2.63) and (2.64) may then be solved for the nodal values of δa

and $\delta a'$. Subsequently, the numerical approximations to the weight functions need to be updated: this is simply a matter of evaluating the appropriate principal value integrals in (2.32) and (2.33): an appropriate method is outlined in Bower and Ortiz (1990).

3. Results and discussion

The perturbation method outlined in the preceding sections may be used to analyse the behaviour of a crack as it propagates through a reinforced brittle solid. Here, we consider an initially straight semi–infinite crack propagating through a brittle matrix material of toughness K_c^{mat}. The matrix is reinforced by a rectangular distribution of tough circular particles, having a spacing L, radius R and toughness K_c^{par}. The ratio of particle radius to spacing is restricted to the range $0 < R/L < 0.25$, to be consistent with the assumptions made in Section 2. The solid is subjected to remote loads, acting so as to induce a mode I stress intensity factor on the crack. The magnitude of the load is parameterised by a remotely applied stress intensity factor K^{∞}, as defined in equation (2.26). Initially, we assume that the particles are perfectly bonded to the matrix material, and fracture in the wake of the crack. The analysis will subsequently be extended to include the effects of debonding between particles and the matrix.

3.1 Perfectly bonded particles

(a) Crack Trapping

Consider first the behaviour of a crack with no pinning particles in its wake, as it meets a row of tough particles. The crack may surmount the row of obstacles in one of two ways. If the toughness of the particles exceeds that of the matrix by only a small amount, they are penetrated by the crack, which propagates through them. Alternatively, if the $K_c^{\mathrm{par}}/K_c^{\mathrm{mat}}$ exceeds a critical value (to be determined), the segments of crack front bowing out between the particles coalesce with one another, and the particles are left intact in the wake of the crack.

The latter behaviour is illustrated on Figs 4 to 6. Fig. 4 shows the shape of one wavelength of the crack front as it propagates around the first row of tough particles, for a particle spacing $L/R = 10$. The front is initially straight, and the wake of the crack is free of pinning particles. When the remote load reaches a magnitude $K^{\infty} = K_c^{\mathrm{mat}}$, the crack starts to propagate through the solid. Parts of the crack front contacting the particles arrest, while the remainder of the front bows out between the particles. Its shape is determined by the condition that $K(s) = K_c^{\mathrm{mat}}$ over propagating regions, while $\delta a(s) = 0$

24

over regions in contact with the tougher material. Due to the change in crack geometry, the stress intensity factor increases over regions of the crack which contact the particles: the resulting distribution of $K(s)$ along the crack front is shown in Fig. 5, at various stages of growth. The results are shown as a function of s/c, where the arc–length s is measured from the point of first contact of the crack front with the obstacle, and c is the arc–length of one period.

The variation of remote stress as the crack propagates around the row of particles is shown in Fig. 6. The load is plotted as a function of $\langle a \rangle / R$: the parameter $\langle a \rangle$ is a measure of the average crack advance, defined as A/L, where A is the area swept by one wavelength of the advancing crack. The load reaches a maximum value of 1.68, and subsequently decreases as areas of the crack front ahead of the particles start to attract one another. As the load decreases, parts of the crack front arrest, and the propagating region progressively diminishes in size to a small zone around the point of coalescence. The finite perturbation method cannot be used to analyse in detail the coalescence of the crack, due to the singular behaviour of the influence function $D(s,t)$, as discussed in section 2. The calculation was stopped when the crack front reached the last profile shown on Fig. 4. However, the remote load must fall to zero at the point of coalescence: since the stress intensity factor is singular where the crack front touches itself, it follows that $K^\infty \to 0$ to satisfy the condition that $K(s) = K_c^{\mathrm{mat}}$ over the propagating region.

In practice, the coalescence of the crack can only be a quasi–static process as shown in Figs 4 and 6 if the solid is subjected to displacement boundary conditions at infinity. Under a steadily increasing remote stress, the configuration of the crack will become unstable when the load reaches the peak value $K^\infty / K_c^{\mathrm{mat}} = 1.68$, and the crack will propagate dynamically until it is arrested by the next row of particles. This behaviour is known as 'pop-in', and has been observed during tests on Alumina by Swanson et al (1987).

Fig. 5 shows that the stress intensity on the region of the crack in contact with the particle reaches a maximum value $K(s) = 2.84$ at $s = 0$. Consequently, if $K_c^{\mathrm{par}} / K_c^{\mathrm{mat}} > 2.84$, the crack bypasses the first row of obstacles, leaving a row of pinning particles: its subsequent propagation is discussed in detail in the next section. Alternatively, if $K_c^{\mathrm{par}} / K_c^{\mathrm{mat}} < 2.84$, the crack front penetrates the particles. In this case, the obstacles fracture, and no bridging particles are formed. The behaviour of a crack breaking through a row of obstacles has been discussed in detail by Gao and Rice (1990). They distinguish between two different cases: stable (or regular), and unstable (irregular) penetration. Stable breakthrough implies that the crack fully penetrates the obstacles before the maximum load is reached. The penetration is unstable if the peak load occurs when the particles are only partially

penetrated.

The maximum load under conditions of stable penetration occurs when the particles are fully penetrated, and the line fraction of the crack front inside the obstacles is a maximum. In this case, the toughening due to trapping can be calculated explicitly, by means of equation (2.26) (Rose, 1975). Since $K(x_2) = K_c^{par}$ for $|x_2| \le R$ and $K(x_2) = K_c^{mat}$ otherwise, we immediately obtain

$$K^\infty = \left\{ (K_c^{mat})^2 + \frac{2R}{L} \left((K_c^{par})^2 - (K_c^{mat})^2 \right) \right\}^{1/2}. \tag{3.1}$$

This expression is exact, and is valid provided the crack can reach the limiting configuration. It gives an upper bound to the toughening due to trapping if the crack bypasses the obstacles, or in the event of unstable penetration.

The shape of the crack at the maximum load may be found using the finite perturbation procedure. The required configuration is determined by the condition that $K(s) = K_c^{par}$ inside the particles, and $K(s) = K_c^{mat}$ outside. This can be satisfied by applying a succession of perturbations such that $\delta K(s) = $ constant for $|x_2| \le R$, and $\delta K(s) = 0$ otherwise. The change in crack geometry may be found by solving equation (2.31) for $\delta a(s)$ at each increment. In this way, the limiting crack configuration may be found for a range of values of K_c^{par} without having to solve explicitly for the load history in each case. A set of results is shown in Fig. 7, for a particle spacing $L/R = 6.67$. It can be seen that if $K_c^{par}/K_c^{mat} > 1.7$, the limiting crack shape cannot be contained within the particles. Under these conditions, the maximum load occurs before the obstacle is fully penetrated. This case has been classified as unstable penetration by Gao and Rice (1990).

If the particles are not fully penetrated at maximum load, equation (3.1) does not apply, and the toughness of the reinforced solid must be calculated numerically. A set of crack profiles for an unstably penetrated obstacle is shown on Fig. 8, for $K_c^{par}/K_c^{mat} = 2.4$ and $L/R = 6.667$. The maximum load was found to be $K^\infty/K_c^{mat} = 1.53$: the corresponding value predicted by equation (3.1) is 1.55. The crack front bowing between the particles joins up on itself after the obstacles are penetrated and a row of partially penetrated particles is left in the wake of the crack. Its subsequent behaviour is discussed below. For small particles ($R/L < 0.18$), the penetrated obstacles fracture before the crack reaches the second row of particles. Under these conditions crack bridging does not contribute to the toughness of the solid: the maximum load occurs while the crack penetrates a single row of obstacles, at the point of instability. However, if $R/L > 0.18$, the penetrated particles remain intact. This situation cannot be modelled exactly using the present method, since

the pinned regions in the crack wake have been assumed to be circular. The penetrated particles are therefore replaced by a row of equivalent circular obstacles, chosen by matching areas.

These calculations have been repeated for a range of values of L/R and K_c^{par}/K_c^{mat}. The results are summarised on Figs. 9 and 10. Fig. 9 shows the mechanism of trapping as a function of the particle toughness and spacing. In the regime marked 'stable penetration,' the crack front fully penetrates the obstacles at the maximum load, and the toughness is given by equation (3.1). For slightly larger values of K_c^{par}/K_c^{mat} in the 'unstable penetration' region, the maximum load occurs before the obstacles are fully penetrated. In the region marked 'unstable bridging', a row of partially penetrated particles remains in the wake, but fractures before the crack front reaches the second row of obstacles. In the 'Partial Bridging' regime, the penetrated particles remain intact and contribute to the toughness of the solid by pinning the crack faces. Finally, if K_c^{par}/K_c^{mat} lies in the area marked 'particles bypassed,' the obstacles are left intact in the wake of the crack. The subsequent behaviour of the crack is discussed in more detail below. Fig. 9 shows that the critical value of K_c^{par}/K_c^{mat} required for bridging particles to be formed increases as L/R is reduced. If there is a large distance between the particles, the crack tends to bow out further. so that the crack is more likely to coalesce ahead of the particles.

The effective toughness of the reinforced material is shown as a function of K_c^{par}/K_c^{mat} on Fig. 10. for various values of L/R. The toughness enhancement due to crack trapping is a monotonically increasing function of K_c^{par}/K_c^{mat} and R/L. Even if no crack bridging takes place, the particles can double toughness of a brittle matrix by trapping the crack front.

(b) Bridging combined with trapping

If the particle toughness lies in the regime marked 'particles bypassed' in Fig. 9. at least one row of bridging particles will be formed in the wake of the crack. This situation is analysed by adding pinning particles behind the crack front and subsequently modifying its shape. as discussed in section 2.2. The propagation of the crack immediately after coalescence cannot be analysed using this procedure, since the calculation assumes that the distance between the pinning particles and the crack front greatly exceeds the particle radius. We therefore resume the analysis after the semi–infinite crack has propagated a short distance beyond the first row of pinning particles. Fig. 12 shows the load as a function of crack advance while the crack bypasses several rows of particles: the dashed portions of

this curve occur during coalescence and have not been calculated explicitly. We have made use of the result that K^∞ must fall to zero at the point of coalescence in order to deduce the probable shape of the $K^\infty - \langle a \rangle$ curve in this regime. Similarly, the dashed regions on Fig. 13 have been deduced by noting that $K^{\text{par}} \to 0$ at coalescence.

A set of crack front profiles during the formation of four pinning particles is shown on Fig. 11. It can be seen that while the crack propagates between the first and second rows of particles, its front remains approximately straight. At this stage, the remote load and the stress intensity around the pinning particles are closely approximated by the results for a straight crack bridged by single row of obstacles, given in equations (2.23) and (2.24). It is straightforward to show that $K^\infty / K_c^{\text{mat}}$ given by (2.23) is a decreasing function of the crack advance b for all L/R. Until the crack front is trapped by the second row of particles, the remote load therefore always decreases as the crack advances. This situation is similar to a crack propagating through a material of decreasing toughness: by differentiating (2.23), the rate of change of effective toughness with crack advance is found to be

$$\frac{\partial K_c^{\text{eff}}}{\partial b} = \frac{-K_c^{\text{mat}} \cosh \pi b/L}{b \sinh \pi b/L (\pi L/8R - L/4\pi b + F(b/L) - 1)^2}, \tag{3.2}$$

where b is the distance from the particles to the crack front, and $F(b/L)$ is defined in (2.25). For b/L in the range $0.5 < b/L < 1.5$, this may be approximated by

$$\frac{\partial K_c^{\text{eff}}}{\partial b} \approx \frac{-6.5 K_c^{\text{mat}}}{b(L/R - 0.93L/b)^2}. \tag{3.3}$$

Bower and Ortiz (1990) have investigated the behaviour of a straight semi–infinite crack propagating through material of decreasing toughness. They have shown that the configuration of the crack is not unique, in that the crack front may not remain straight. In particular, small imperfections in the geometry of the crack containing a critical wavelength c_{crit} are likely to grow as the crack advances. The critical wavelength is given by

$$c_{\text{crit}} = -\frac{\pi K_c^{\text{eff}}}{\partial K_c^{\text{eff}} / \partial b}. \tag{3.4}$$

For the case in hand

$$c_{\text{crit}} \approx \frac{b(L/R - 0.93L/b)^2}{6.5}. \tag{3.5}$$

This result suggests that shortly after the crack bypasses a row of obstacles (b small), the crack front may adopt a wavy configuration, and advance by forming a series of short wavelength 'fingers'. However, for the range of L/R considered here, $c_{\text{crit}} > L$ for $b \approx L$. The present analysis constrains the crack front to remain periodic with wavelength L, so

28

once the distance from the bridging particles to the crack front is comparable to the obstacle spacing, the crack front remains approximately straight.

The stress intensity factor on the bridging particles is plotted as a function of crack advance on Fig. 13, for $L/R = 10$. While the crack propagates between the first and second rows, K^{par}/K_c^{mat} is closely approximated by the result for a straight crack, given in equation (2.23). The particles fracture when $K^{par} = K_c^{par}$: this condition may be used to calculate the value of K_c^{par} required for the obstacles to remain intact until the crack front reaches the second row of obstacles. Putting $b \approx L$ in (2.23) we find that:

$$\frac{K_c^{par}}{K_c^{mat}} \approx \sqrt{\frac{L}{2R}} \frac{1}{\pi/4 - 0.729R/L}. \tag{3.6}$$

For large L/R, the particle toughness for the pinning regions to be stable exceeds the critical value required for the crack to bypass the particles. For example, if $L/R = 10$, the crack bypasses the first row of particles if $K_c^{par}/K_c^{mat} > 2.79$. Equation (3.6) shows that the particles fracture before the crack front reaches the second row of obstacles unless $K_c^{par}/K_c^{mat} > 3.14$. If K_c^{par}/K_c^{mat} lies between 2.79 and 3.14, the crack bypasses the first row of obstacles, which subsequently fractures while the crack advances towards the second row.

If K_c^{par}/K_c^{mat} exceeds 3.14, the bridging particles remain intact until the crack is trapped by the second row of obstacles. At this point, the remote load starts to increase while the crack bows out between the obstacles, as shown in Fig. 12. At the same time, the stress intensity on the bridging particles increases rapidly, Fig 13. Eventually, K^∞ exceeds the maximum value reached while bypassing the first row of obstacles: for $L/R = 10$, the critical value $K^\infty = 1.43$ is reached when $\langle a \rangle/R = 11$. At this point $K_c^{par}/K_c^{mat} = 3.54$. Consequently, if the particle toughness lies in the range $2.84 < K^{par}/K_c^{mat} < 3.54$, the maximum load occurs at the instant when the crack bypasses the first row of particles. Although bridging particles are subsequently formed, they fracture at a lower load, and do not contribute to the toughness of the reinforced solid. This behaviour will be referred to as 'unstable bridging.' The range of K_c^{par}/K_c^{mat} for unstable bridging to occur is shown as a function of R/L on Fig. 9. In this regime, variations in particle toughness produce no change in the effective toughness of the reinforced material.

A similar argument applies to partially penetrated obstacles in the wake of the crack. If the obstacles are small, they fracture before the crack front reaches the second row of particles. Large particles remain intact for long enough to contribute to the toughness of the reinforced solid by pinning the crack faces.

The behaviour of the crack as it bypasses further rows of particles is similar. As the particle toughness is increased, several stable rows of pinning particles may form in the wake of the crack. Fig. 9 shows the number of bridging particles as a function of K_c^{par}/K_c^{mat} and L/R. In the regions marked 'unstable bridging,' an additional row of particles is formed but fractures without improving the toughness. Under these conditions, the maximum load is reached at the point where the crack just bypasses a new row of obstacles. Otherwise, the maximum load is reached when the row of bridging particles furthest from the crack front fractures. In the steady state, bridging particles fracture at the same rate in the wake of the crack as they are formed at its front. The load fluctuates considerably as the crack propagates: this is a consequence of the periodicity of the distribution of particles. Smaller variations in load would be expected if the particle distribution were random.

The maximum remote load has been plotted as a function of the particle toughness on Fig. 14, for various values of R/L: K^∞ may be interpreted as the effective toughness of the reinforced solid. It can be seen that for $K_c^{par}/K_c^{mat} > 7$, K^∞/K_c^{mat} varies linearly with K_c^{par}/K_c^{mat}, and is closely approximated by the relation:

$$\frac{K^\infty}{K_c^{mat}} = 3.09 \frac{R}{L} \frac{K_c^{par}}{K_c^{mat}}. \tag{3.7}$$

It is not difficult to explain this behaviour. Consider a straight, semi–infinite crack propagating through a material of toughness K_c^{mat} which contains a rectangular distribution of particles, toughness K_c^{par}, radius R and spacing L. As the crack propagates a distance L, the work done per unit area in fracturing the particles varies as $\pi R^2 (K_c^{par})^2/L^2$, while the work done in cleaving the matrix is proportional to $(1 - \pi R^2/L^2)(K_c^{mat})^2$. It follows that the effective toughness of the composite material is given by

$$\frac{K_c^{eff}}{K_c^{mat}} = \sqrt{1 + \pi \frac{R^2}{L^2} \left(\frac{(K_c^{par})^2}{(K_c^{mat})^2} - 1 \right)}. \tag{3.8}$$

Expanding (3.8) for $K_c^{par}/K_c^{mat} \gg 1$ shows that

$$\frac{K_c^{eff}}{K_c^{mat}} \approx \sqrt{\pi} \frac{R}{L} \frac{K_c^{par}}{K_c^{mat}}, \tag{3.9}$$

giving the linear behaviour observed in Fig. 14. The constant coefficients in (3.7) and (3.9) differ, since equation (3.9) gives the average effective toughness, while (3.7) gives the maximum value, and includes the transient effect of crack trapping.

It is evident that adding small quantities of tough particles to a brittle material can substantially improve its toughness. While the toughness enhancement due to crack tip

microcracking or deflection is modest at best, the present analysis shows that crack trapping combined with bridging can improve the fracture toughness by a factor of 5 or more. However, several criteria must be satisfied in order to achieve these levels of toughness. The particles must be perfectly bonded to the matrix material, and their toughness must be of the order of 10 times that of the matrix. This may be the case in ceramics and glasses reinforced by metallic particles, but is unlikely in monolithic ceramics. The analysis also shows that only a very small number of perfectly pinned particles are likely to form in the wake of a crack. Even if $K_c^{\mathrm{par}}/K_c^{\mathrm{mat}} \approx 15$, only 10 particles remain intact for $L/R = 20$.

(c) Comparison with experiments

Krstic et al (1981) have measured the toughness of glass reinforced by partially oxidized aluminium particles. The assumptions made in the present analysis satisfy the conditions of their experiments. The oxide layer on the particles forms a strong bond with the Al_2O_3 in the glass, and the elastic constants and thermal expansion coefficient of both materials are closely matched. The measured toughness (normalised by K_{IC} for pure glass) is shown on Fig. 14, as a function of the volume fraction of particles, V_f.

In order to compare experimental and theoretical results, it is necessary to relate the particle spacing used in the analysis to an equivalent volume fraction of randomly distributed particles. It is straightforward to show that if a plane cuts through a random distribution of spheres, the area fraction of the plane inside the particles is equal to their volume fraction. Matching area fractions for the periodic and random distributions, we find that

$$\frac{R}{L} = \sqrt{\frac{V_f}{\pi}}. \tag{3.10}$$

Using (3.10), equation (3.7) may be expressed in terms of V_f as

$$\frac{K^\infty}{K_c^{\mathrm{mat}}} = 1.74\sqrt{V_f}\frac{K_c^{\mathrm{par}}}{K_c^{\mathrm{mat}}}. \tag{3.11}$$

This result has been plotted on Fig. 14. Taking $K_c^{\mathrm{par}}/K_c^{\mathrm{mat}} = 11$ gives excellent agreement between theory and experiment. However, this choice of particle toughness is arbitrary, and is probably an underestimate. With higher values of K_c^{par}, equation (3.11) overestimates the toughness of the composite: this is to be expected, since the periodic particle distribution used in the theory overestimates the toughness enhancement due to crack trapping by a random distribution.

31

The R–curve behaviour of a monolithic ceramic has been measured by Vekinis et al (1990). Their results are shown on Fig. 16. The toughness reaches a steady state after 11mm of crack growth, suggesting that the length of the bridged zone exceeds 2000 grain diameters. According to the present analysis, particles would need to be over 100 times tougher than the matrix to remain intact over this length: equation (3.7) would then predict a corresponding toughness enhancement of the order of a factor of 30. It is clearly not reasonable to assume that grains remain perfectly bonded to the matrix in monolithic ceramics. The R–curve behaviour observed in Fig. 16 is more likely to be caused by frictional crack bridging. This issue is addressed in the next section.

3.2 Frictional crack bridging

If particles are weakly bonded to the matrix, the interface between particles and matrix fails before the particles fracture, so that they are pulled out in the wake of the crack. The idealised model of this process was discussed in section 2.4. We assume each grain to be cylindrical, having a radius R and height δ_{crit}, with its axis perpendicular to the plane of the crack. The particles are assumed to be sufficiently tough so as not to be penetrated by the crack. The foremost row of particles remains bonded to the matrix, so that the effects of crack trapping are as discussed in the preceding sections: the particles are bypassed by the crack front and remain intact in the wake of the crack. The particles remain perfectly bonded until the pinning force on a row of grains exceeds $P_0 = \pi R \delta_{\text{crit}} f \sigma_r$, at which point they start to be pulled free from the matrix. Thereafter, the pinning–force is related to the crack opening displacement by equation (2.49).

The toughening due to frictional crack bridging can be expressed in terms of four non–dimensional groups

$$\frac{K^\infty}{K_c^{\text{mat}}} = F\left(\frac{P_0 \delta_{\text{crit}}}{L^2 \Lambda (K_c^{\text{mat}})^2}, \frac{R}{L}, \frac{L^2 \delta_{\text{crit}}}{\Lambda R P_0}, \frac{\delta_{\text{crit}}}{R} \right). \tag{3.12}$$

Here, the first group is the ratio of the frictional energy dissipation rate to the critical energy release rate of the matrix material. This is equivalent to the parameter $(K_c^{\text{par}}/K_c^{\text{mat}})^2$ in the case of perfectly pinned particles. The second group, L/R is a measure of the volume fraction of particles, as before. The third group is new, and requires some explanation. The ratio $P_0/L^2 \delta_{\text{crit}}$ is a measure of the slope of the $P - \delta$ curve during pull–out of the particles. In contrast, ΛR is related to the compliance of the faces of the crack under a distribution of pressure. Thus, the third dimensionless group in (3.12) is a measure of the ratio of the compliance of the frictional pinning force–pull out curve to the elastic compliance of

32

the crack faces. This parameter has an important influence on the length of the bridging zone. The last dimensionless group governs the three–dimensional shape of the particles: for simplicity, we will assume that $\delta_{crit}/R = 2$ for all calculations here.

Typical values for the parameters in this model are given in Table 1, chosen to be representative of alumina. Parameters such as the grain size R and the elastic constants are easily determined, but the parameters governing frictional–pull out can only be estimated. Here, we have assumed that the compressive residual stress pinning each grain to the matrix $\sigma_r \approx 120$MPa. Stresses of this magnitude have been predicted by Ortiz and Suresh (1989) and measured by Blendel and Coble (1982). The coefficient of friction has been taken as 0.6. For a grain size of the order of 4μm, this leads to a maximum pull–out force $P_0 \approx 0.008$N.

Fig. 15 shows the predicted R–curve behaviour due to frictional crack bridging, for an appropriate value of $P_0\delta_{crit}/L^2\Lambda(K_c^{mat})^2$. The fluctuation in load as the crack bypasses individual rows of particles has not been shown in Fig 15: we have assumed that the solid is subjected to a monotonically increasing remote stress, and ignored unstable crack growth. The effective toughness was calculated by adding rows of particles to the wake of the crack, and then finding the maximum value of remote load as the crack bypasses the next row. This procedure gives an upper bound to the combined toughening due to bridging and trapping.

The R–curve initially rises steeply as the crack bypasses the first row of particles. The crack growth during the initial increase in stress is of the order of the grain size, so it is unlikely that this part of the curve could be detected experimentally. Instead, the initial toughness of the material would appear to be greater than that of the matrix. The initial toughness of alumina measured by Vekinis et al (1990) (see Fig. 15) is of the order of 3.3 MPa$\sqrt{m}$: the inherent matrix toughness to give this initial value is 1.9MPa$\sqrt{m}$. The equivalent surface energy of 6 Jm^{-2} is in good agreement with measured values for Alumina. Crack trapping can therefore account for the observed discrepancy between the surface energy and fracture toughness of polycrystalline alumina. However, the origin of the tough grains responsible for trapping is yet to be determined with certainty.

Once the particles have been bypassed, they remain perfectly bonded to the matrix for only a short time. For the parameters used here, no more than a single row was found to remain fully pinned The remaining particles pull out in the wake of the crack. As a result, the toughness enhancement due to bridging is greatly reduced: although over 500 particles remain in the bridged zone, the toughness enhancement is only of the order of 20-30%. The predicted increase in toughness is in good agreement with the experimentally

measured values shown in Fig. 15; furthermore, the measured and calculated length of the bridging zones are comparable.

The effects of varying the parameters $P_0 \delta_{\mathrm{crit}} / L^2 \Lambda (K_c^{\mathrm{mat}})^2$, R/L and $L^2 \delta_{\mathrm{crit}} / \Lambda R P_0$ are shown in Figs. 16 to 18. Fig. 16 shows the influence of the frictional energy dissipation on the toughness increase due to bridging ΔK_R, while Fig. 17 shows the variation of the length of the bridged zone. The compliance ratio $L^2 \delta_{\mathrm{crit}} / \Lambda R P_0$ has little influence on the toughness: varying this parameter from 10×10^3 to 100×10^3 produced only a 5% change in toughness. However, the length of the bridged zone is controlled by the compliance ratio, as seen on Fig. 18. This suggests that the toughness is mainly determined by the area under the pinning force–pull out curve, and is not greatly affected by its shape.

The influence of grain size on the toughness of Alumina is an intriguing feature of the experimental study by Vekinis et al. (1990). The toughness was observed to increase with grain size, but the length of the bridging zone decreased. The effects of variations in grain size may be calculated using the theoretical model developed here. From equation (2.50), we find that P_0 varies as R^2. If the volume fraction of tough grains (parameterised by L/R) remains fixed, and the aspect ratio δ_{crit}/R is unchanged, then the first dimensionless group in (3.12) varies linearly with grain size R, while the other groups are unaffected. The effect of grain size on toughness and bridging length may therefore be deduced from Figs. 16 and 17. The measured toughness agrees well with the calculated values, but the theory predicts that the bridging length increases with grain size, contrary to experimental observations.

The reason for this discrepancy is not clear. It is not difficult to adjust the parameters in the theoretical model to produce a simultaneous increase in toughness and decrease in bridging length: for example, the compliance ratio or the aspect ratio of the grains could be chosen appropriately. The annealing process used to increase the grain size may alter the residual stress distribution in the solid, or change the interfacial toughness. This influences the number of grains left intact in the wake of the crack. However, the volume fraction and aspect ratio of tough grains are difficult to measure, and no data are available at present to allow a complete study.

4. Conclusions

A three–dimensional model has been developed to calculate the toughness of a brittle material reinforced by tough particles. The reinforced material has been idealised as an

elastically homogeneous solid, containing a regular distribution of tough circular particles. The analysis predicts the behaviour of an initially straight, planar, semi–infinite crack as it propagates through the solid under a uniform remote stress. The particles may inhibit fracture by three mechanisms: firstly, the particles trap the crack front, causing it to bow out between them. Secondly, the particles may remain intact in the wake of the crack, thereby pinning its faces and carrying part of the load. Finally, the particles may debond from the matrix and dissipate energy in frictional sliding as they are pulled out in the wake of the crack. All three mechanisms have been investigated.

The results for particles perfectly bonded to the matrix are summarised in Figs. 9 and 10. Fig. 9 shows the number of pinning particles that form in the wake of the crack, as a function of the obstacle spacing and toughness. If K_c^{par} exceeds K_c^{mat} by only a small amount, the obstacles are penetrated by the crack front, and no bridging particles are formed. Crack trapping is then the only toughening mechanism. If the particle toughness exceeds a critical value, they remain intact in the wake of the crack. The toughness enhancement due to combined crack trapping and bridging is shown in Fig. 10. Asymptotic expressions have been found for the toughness of the reinforced solid, both for particles whose toughness is comparable to that of the matrix, and also for particles much stronger than the matrix. If $K_c^{\mathrm{par}} < 3K_c^{\mathrm{mat}}$, the obstacles are penetrated by the crack front, and no bridging particles form in the crack wake. Under these conditions, the toughness of the reinforced solid is given by Rose (1975) as

$$\frac{K^\infty}{K_c^{\mathrm{mat}}} = \left\{ 1 + \frac{2R}{L} \left(\frac{(K_c^{\mathrm{par}})^2}{(K_c^{\mathrm{mat}})^2} - 1 \right) \right\}^{1/2} . \tag{4.1}$$

Conversely, if $K_c^{\mathrm{par}}/K_c^{\mathrm{mat}} > 7$, the results are closely approximated by the simple relation

$$\frac{K^\infty}{K_c^{\mathrm{mat}}} = 3.09 \frac{R}{L} \frac{K_c^{\mathrm{par}}}{K_c^{\mathrm{mat}}}. \tag{4.2}$$

Equation (4.1) applies for all ratios of R/L, but (4.2) applies only for $R/L < 0.25$

Two important conclusions may be drawn from the theoretical results. Firstly, crack trapping and bridging are very effective toughening mechanisms. While the toughness enhancement due to crack tip microcracking or crack deflection is modest at best, crack trapping combined with bridging can improve toughness by a factor of 5 or more. Secondly, the particle toughness must exceed that of the matrix by a considerable margin if pinning particles are to be formed. If $K_c^{\mathrm{par}}/K_c^{\mathrm{mat}} < 3$, the particles are always penetrated by the crack front. Even if $K_c^{\mathrm{par}}/K_c^{\mathrm{mat}} \approx 15$, only 10 rows of obstacles remain intact in the wake of the crack.

It is reasonable to assume that particles remain perfectly bonded to the matrix in glasses reinforced by metallic particles, and the theoretical results are in good agreement with the experimental data of Krstic et al (1981) on reinforced glass. However, the assumption of perfect pinning does not predict accurately the toughness of monolithic ceramics.

In materials where the particles are weakly bonded to the matrix, the particles remain intact and are pulled out in the wake of the crack. This has been modelled by assuming that the particles remain perfectly bonded to the matrix until the pinning force exceeds a critical value P_0, whereupon the particles start to separate from the matrix. During pull-out, the pinning force decreases linearly with crack opening displacement. Under these conditions the toughness enhancement due to trapping remains the same as for perfectly pinned particles, but the toughening due to bridging is reduced. The predicted R–curve for a typical ceramic is shown in Fig. 15. The improvement in toughness due to frictional bridging is only of the order of 20%, although over 500 rows of grains remain intact in the bridged zone. The R–curve behaviour of the reinforced solid is strongly dependent on the strength of the bond between particles and matrix. If the bond is strong, the toughness increases rapidly as the crack advances, and the maximum toughness is reached when only a few bridging particles form in the crack wake. In contrast, when particles are pulled out in the crack wake, the R–curve increases only slowly with crack advance. Under these conditions several hundred bridging particles may form before the maximum toughness is reached: this requires a large crack extension.

The calculated toughening due to frictional crack bridging is in good agreement with the experimental measurements in alumina by Vekinis et al (1990). The influence of crack trapping and bridging can account for the discrepancy between surface energy and fracture toughness observed in polycrystalline ceramics. However, a key issue has not been addressed by the present analysis. We have assumed that some grains in the ceramic are tougher than others: the origin of the tough regions is not clear. There are several possible explanations. Compressive residual stresses are set up in polycrystalline ceramics due to the thermal and elastic anisotropy of the grains. Evans et al (1977) have suggested that grains in a state of residual compression are less likely to be fractured by a growing crack and may be left behind as bridging particles. A second possibility is that the crack may be deflected along the interface between grains and remain trapped inside the interface. These are promising areas for future research.

Appendix A

This section derives the expressions for increments in the influence functions $\delta H(s, \mathbf{x})$ and $\delta D(s, t)$ given in equations (2.32) and (2.33). Rice (1987) gives a detailed discussion of the procedure necessary to update these functions. Formally, if the crack front C is advanced by an amount $\delta a(\lambda)$ to a new configuration $\bar{C}$, then δH and δD follow from:

$$\delta H(s, \mathbf{x}) = \frac{1}{2\pi} \int_C H(\lambda, \mathbf{x}) D(s, \lambda) \delta a(\lambda) \, d\lambda, \qquad (A1)$$

$$\delta D(s, t) = \frac{1}{2\pi} \int_C D(s, \lambda) D(\lambda, t) \delta a(\lambda) \, d\lambda. \qquad (A2)$$

However, $D(s, t)$ varies as $(t - s)^{-2}$ as $t \to s$. Consequently, the integrals in (A1) and (A2) are undefined unless $\delta a(\lambda) \to 0$ at $\lambda \to s$, in which case they are defined in the principal value sense. Rice (1987) has pointed out that the integrals may be regularised for a general perturbation by exploiting the known behaviour of the crack under a self–similar expansion, rotation and translation. The necessary steps have been discussed by Bower and Ortiz (1990).

In order to apply (A1) to a general crack advance, it is first necessary to apply a combination of a self–similar expansion q, a translation $\delta \mathbf{x}$ and a rotation $\delta \omega$ to the crack front so as to set up a reference configuration C^{ref}. The reference configuration must be chosen so that the point $\mathbf{x}$ is common to both C and C^{ref}, but the crack advance from C^{ref} to $\bar{C}$ satisfies $\delta a^{\text{ref}}(s) = 0$. It is straightforward to show that an appropriate combination of expansion, translation and rotation are given by:

$$q = 1 - \delta a(s) \frac{[\mathbf{x} - \mathbf{z}(s)] \cdot \mathbf{n}(s)}{[\mathbf{x} - \mathbf{z}(s)] \cdot [\mathbf{x} - \mathbf{z}(s)]}, \qquad (A3)$$

$$\delta \omega = \delta a(s) \frac{[(\mathbf{z}(s) - \mathbf{x}) \times \mathbf{k}] \cdot \mathbf{n}(s)}{[\mathbf{x} - \mathbf{z}(s)] \cdot [\mathbf{x} - \mathbf{z}(s)]}, \qquad (A4)$$

$$\delta \mathbf{x} = (1 - q)\mathbf{x} - \mathbf{x} \times \mathbf{k} \delta \omega, \qquad (A5)$$

to first order in $\delta a(s)$. The resulting reference crack front displacement is

$$\delta a^{\text{ref}}(\lambda) = \delta a(\lambda) - [(q - 1)(\mathbf{z}(\lambda) - \mathbf{x}) + \delta \omega(\mathbf{z}(\lambda) - \mathbf{x}) \times \mathbf{k}] \cdot \mathbf{n}(\lambda). \qquad (A6)$$

In setting up the reference configuration, $H(s, \mathbf{x})$ changes by an amount

$$\delta H(s, \mathbf{x}) = H(s, \mathbf{x}) \left(\frac{1}{q^{3/2}} - 1 \right) \qquad (A7)$$

$$\approx \frac{3}{2} \delta a(s) H(s, \mathbf{x}) \frac{[\mathbf{x} - \mathbf{z}(s)] \cdot \mathbf{n}(s)}{[\mathbf{x} - \mathbf{z}(s)] \cdot [\mathbf{x} - \mathbf{z}(s)]}, \qquad (A8)$$

37

since $H(qs, q\mathbf{x})$ scales as $H(s, \mathbf{x})/q^{3/2}$ under uniform expansion, and is invariant to translation and rotation. Adding this contribution to equation (A1), replacing $\delta a(\lambda)$ with $\delta a^{\text{ref}}(\lambda)$ and performing some simple vector manipulations on the result leads to the expression quoted in equation (2.32).

A similar procedure may be used to extend (A2) to general crack advance. This time, it is necessary to set up a reference configuration that satisfies $\delta a^{\text{ref}}(s) = \delta a^{\text{ref}}(t) = 0$. Bower and Ortiz (1990) give the necessary expansion, rotation and translation as

$$q = 1 + \frac{[\delta a(t)\mathbf{n}(t) - \delta a(s)\mathbf{n}(s)] \cdot [\mathbf{z}(t) - \mathbf{z}(s)]}{[\mathbf{z}(t) - \mathbf{z}(s)] \cdot [\mathbf{z}(t) - \mathbf{z}(s)]}, \qquad (A9)$$

$$\delta\omega = \frac{[\delta a(s)\mathbf{n}(s) - \delta a(t)\mathbf{n}(t)] \cdot [(\mathbf{z}(s) - \mathbf{z}(t)) \times \mathbf{k}]}{[\mathbf{z}(s) - \mathbf{z}(t)] \cdot [\mathbf{z}(s) - \mathbf{z}(t)]}, \qquad (A10)$$

$$\delta\mathbf{x} = \delta a(t)\mathbf{n}(t) - (q-1)[\mathbf{x}(t) - \mathbf{x}(t)] \times \mathbf{k}\delta\omega, \qquad (A11)$$

and the resulting reference crack front displacement is

$$\delta a^{\text{ref}}(\lambda) = \delta a(\lambda) - [(q-1)\mathbf{z}(\lambda) + \delta\mathbf{x} + \mathbf{z}(\lambda) \times \mathbf{k}\delta\omega] \cdot \mathbf{n}(\lambda). \qquad (A12)$$

Since $D(qs, qt)$ scales as $D(s, t)/q^2$ under uniform expansion, and is invariant to rotation and translation, the change in $D(s, t)$ in setting up the reference configuration is

$$\delta D(s, t) = D(s, t)\left(\frac{1}{q^2} - 1\right) \qquad (A13)$$

$$\approx -2D(s, t)\frac{[\delta a(t)\mathbf{n}(t) - \delta a(s)\mathbf{n}(s)] \cdot [\mathbf{z}(t) - \mathbf{z}(s)]}{[\mathbf{z}(t) - \mathbf{z}(s)] \cdot [\mathbf{z}(t) - \mathbf{z}(s)]}. \qquad (A14)$$

Including this contribution in equation (A2), replacing δa by δa^{ref} and simplifying the result leads to the expression given in equation (2.33).

Appendix B

In this section, the steps necessary to derive equations (2.35) to (2.38) from (2.29) to (2.32) are outlined.

Finding $\delta U(\mathbf{x})$ (equation (2.35)) is straightforward. From (2.29), we may write

$$\delta U(\mathbf{x}) = \frac{\delta K^\infty}{K^\infty} U(\mathbf{x}) + \frac{1}{2} \int_{-\infty}^\infty K_0(s) H(s, \mathbf{x}) \delta a(s) \, ds, \qquad (B1)$$

where the first term gives the contribution to δU due to a change in the remote load, and the second term gives the effect of a change in the geometry. Since the crack geometry and the crack advance are periodic, this may be re-written as an integral over one wavelength of the crack

$$\delta U(\mathbf{x}) = \frac{1}{2} \int_{-c/2}^{c/2} \sum_{m=-\infty}^{+\infty} K_0(s) H(s + mc, \mathbf{x}) \delta a(s) \, ds. \qquad (B2)$$

Finally, noting that $H(s + mc, \mathbf{x}) = H(s, \mathbf{x} - mL\mathbf{j})$ and using (2.18), we deduce that

$$\delta U(\mathbf{x}) = \frac{1}{2} \int_{-c/2}^{c/2} K_0(s) \mathbf{H}(s, \mathbf{x}) \delta a(s) \, ds. \qquad (B3)$$

The expression for $\delta K_0(s)$ follows in much the same way. Begin by writing:

$$\delta K_0(s) = \frac{\delta K^\infty}{K^\infty} + \int_{-\infty}^\infty K_0(\lambda) D(s, \lambda)[\delta a(\lambda) - \delta a(s)\mathbf{n}(\lambda) \cdot \mathbf{n}(s)] \, d\lambda. \qquad (B4)$$

This may then be expressed as an integral over one wavelength as

$$\delta K_0(s) = \frac{\delta K^\infty}{K^\infty} + \int_{-c/2}^{+c/2} K_0(\lambda) \sum_{m=-\infty}^\infty D(\lambda + mc, t)[\delta a(\lambda) - \delta a(s)\mathbf{n}(\lambda) \cdot \mathbf{n}(s)] \, d\lambda. \qquad (B5)$$

Finally, using (2.39), this becomes

$$\delta K_0(s) = \frac{\delta K^\infty}{K^\infty} K_0(s) + \frac{1}{2\pi} \int_{-c/2}^{c/2} K_0(s) \mathbf{D}(\lambda, s)[\delta a(\lambda) - \delta a(s)\mathbf{n}(\lambda) \cdot \mathbf{n}(s)] \, d\lambda, \qquad (B6)$$

Consider next updating $\mathbf{H}(\mathbf{s}, \mathbf{x})$. Using the definition (2.19), $\delta \mathbf{H}$ may be expressed in terms of δH:

$$\delta \mathbf{H}(s, \mathbf{x}) = \sum_{m=-\infty}^{+\infty} \delta H(s, \mathbf{x} + mL\mathbf{j}). \qquad (B7)$$

39

Now, δH is given by (2.32). It is convenient to split (2.32) into a periodic and a non–periodic part, as

$$\delta H(s, \mathbf{x}) = \frac{1}{2\pi} \int_{-\infty}^{\infty} H(\lambda, \mathbf{x}) D(\lambda, s) [\delta a(\lambda) - \delta a(s) \mathbf{n}(\lambda) \cdot \mathbf{n}(s)]$$
$$+ \quad \delta a(s) \Psi(s, \mathbf{x}), (B8)$$

where

$$\Psi(s, \mathbf{x}) = \frac{1}{2\pi} \int_{-\infty}^{+\infty} H(\lambda, \mathbf{x}+) D(\lambda, s)$$
$$\left\{ \mathbf{n}(\lambda) \cdot \mathbf{n}(s) - \frac{[\mathbf{x} - \mathbf{z}(\lambda)] \cdot [\mathbf{x} - \mathbf{z}(s)]}{[\mathbf{x} - \mathbf{z}(s)] \cdot [\mathbf{x} - \mathbf{z}(s)]} [\mathbf{n}(\lambda) \cdot \mathbf{n}(s)] \right.$$
$$\left. - \frac{[\mathbf{x} - \mathbf{z}(\lambda)] \times [\mathbf{x} - \mathbf{z}(s)] \cdot \mathbf{k}}{[\mathbf{x} - \mathbf{z}(s)] \cdot [\mathbf{x} - \mathbf{z}(s)]} [\mathbf{n}(\lambda) \times \mathbf{n}(s)] \cdot \mathbf{k} \right\} d\lambda$$
$$+ \frac{3}{2} H(s, \mathbf{x}) \frac{[\mathbf{x} - \mathbf{z}(s)] \cdot \mathbf{n}(s)}{[\mathbf{x} - \mathbf{z}(s)] \cdot [\mathbf{x} - \mathbf{z}(s)]}. \tag{$B9$}$$

Using (B7), and rewriting the integrals over a single wavelength, the expression for $\delta\mathbf{H}$ becomes

$$\delta\mathbf{H}(s, \mathbf{x}) = \frac{1}{2\pi} \int_{-c/2}^{c/2} \sum_{n=-\infty}^{+\infty} \sum_{m=-\infty}^{+\infty} H(\lambda + nc, \mathbf{x} + mL\mathbf{j}) D(\lambda + nc, s) [\delta a(\lambda) - \delta a(s) \mathbf{n}(\lambda) \cdot \mathbf{n}(s)] \, d\lambda$$
$$+ \delta a(s) \sum_{m=-\infty}^{+\infty} \Psi(s, \mathbf{x} + mL\mathbf{j}). \tag{$B10$}$$

By defining two new functions:

$$\mathbf{D}(s, \lambda) = \sum_{n=-\infty}^{\infty} D(\lambda + nc, s), \tag{$B11$}$$

$$\mathbf{\Psi}(s, \mathbf{x}) = \sum_{n=-\infty}^{+\infty} \sum_{m=-\infty}^{+\infty} \Psi(s + nc, \mathbf{x} + mL\mathbf{j}), \tag{$B12$}$$

and writing the integral in (B9) as a sum over successive wavelengths, we obtain the result given in (2.38).

Finally, it is necessary to find a procedure for updating $\mathbf{G}(\mathbf{x}^{(n)}, \mathbf{x}^{(k)})$. Begin with the definition in (2.14)

$$\mathbf{G}(\mathbf{x}^{(n)}, \mathbf{x}^{(k)}) = \begin{cases} \dfrac{1}{4R} + \dfrac{1}{2\pi^2 x_1^{(n)}} + \displaystyle\sum_{\substack{m=-\infty \\ m \neq 0}}^{\infty} G(\mathbf{x}^{(n)} + mL\mathbf{j}, \mathbf{x}^{(n)}), & n = k; \\[4mm] \displaystyle\sum_{m=-\infty}^{\infty} G(\mathbf{x}^{(k)} + mL\mathbf{j}, \mathbf{x}^{(n)}), & n \neq k. \end{cases} \tag{$B13$}$$

40

Each term in (B13) may now be updated in turn. Consider first the case $n \neq k$. From (2.30), we immediately obtain

$$\delta \mathbf{G}(\mathbf{x}^{(n)}, \mathbf{x}^{(k)}) = \sum_{m=-\infty}^{+\infty} \frac{1}{2} \int_{-\infty}^{+\infty} H(\lambda, \mathbf{x}^{(k)} + mL\mathbf{j}) H(\lambda, \mathbf{x}^{(n)}) \delta a(\lambda) \, d\lambda, \qquad n \neq k, \quad (B14)$$

which, written as an integral over one wavelength of the crack is

$$\delta \mathbf{G}(\mathbf{x}^{(n)}, \mathbf{x}^{(k)}) = \frac{1}{2} \int_{-c/2}^{+c/2} \mathbf{H}(\lambda, \mathbf{x}^{(k)}) \mathbf{H}(\lambda, \mathbf{x}^{(n)}) \delta a(\lambda) \, d\lambda, \qquad n \neq k. \qquad (B15)$$

Consider now the case $n = k$. The infinite sum may be updated using a similar procedure as for the case $n \neq k$, leaving the term $1/4R + 1/(2\pi^2 x_1^{(n)})$. To update this contribution, it is necessary to return to the original derivation of $\mathbf{G}$. Recall that this term represents the approximate solution to the integral equation

$$0 = U(\mathbf{x}) + \int_{\Omega} G(\boldsymbol{\xi}, \mathbf{x}) p(\boldsymbol{\xi}) d\boldsymbol{\xi}, \qquad (B16)$$

which is an expression for the the pressure required to pin a single circular region on the crack. To update the solution, we therefore need to solve

$$0 = U(\mathbf{x}) + \delta U(\mathbf{x}) + \int_{\Omega} \{G(\boldsymbol{\xi}, \mathbf{x}) + \delta G(\boldsymbol{\xi}, \mathbf{x})\} (p(\boldsymbol{\xi}) + \delta p(\boldsymbol{\xi})) \, d\boldsymbol{\xi}. \qquad (B17)$$

Neglecting second order terms and using (B16), this becomes

$$0 = \delta U(\mathbf{x}) + \int_{\Omega} \delta G(\boldsymbol{\xi}, \mathbf{x}) p(\boldsymbol{\xi}) + G(\boldsymbol{\xi}, \mathbf{x}) \delta p(\boldsymbol{\xi}) \, d\boldsymbol{\xi}. \qquad (B18)$$

Substituting for δG from (2.30) then gives

$$0 = \delta U(\mathbf{x}) + \int_{\Omega} \left\{ \frac{1}{2} \int_C H(s, \boldsymbol{\xi}) H(s, \mathbf{x}) \delta a(s) \, ds \right\} p(\boldsymbol{\xi}) + G(\boldsymbol{\xi}, \mathbf{x}) \delta p(\boldsymbol{\xi}) \, d\boldsymbol{\xi}. \qquad (B19)$$

In the spirit of the analysis presented in section 1, we now assume that $R << L$ and write

$$H(s, \boldsymbol{\xi}) \approx H(s, \mathbf{x}), \qquad (B20)$$

accurate to lowest order in R/L. This leads to the following integral equation for $\delta p(\boldsymbol{\xi})$

$$0 = \delta U(\mathbf{x}) + P \frac{1}{2} \int_C H(s, \boldsymbol{\xi}) H(s, \mathbf{x}) \delta a(s) \, ds + \int_{\Omega} G(\boldsymbol{\xi}, \mathbf{x}) \delta p(\boldsymbol{\xi}) \, d\boldsymbol{\xi}, \qquad (B21)$$

where P is the resultant of the pressure distribution $p(\boldsymbol{\xi})$, as defined in section 2. Comparison with (B16) shows that the solution to this equation must have the form given in eqution (2.8). The distribution of pressure on each pinning particle therefore remains constant as the crack front is perturbed, only its magnitude is affected. Furthermore, the second term in (B21) clearly represents the change in the $1/4R + 1/2\pi^2 x_1^{(n)}$ term in $\mathbf{G}$. Conveniently, combining terms in $\delta \mathbf{G}$ shows that

$$\delta \mathbf{G}(\mathbf{x}^{(n)}, \mathbf{x}^{(k)}) = \frac{1}{2} \int_{-c/2}^{c/2} \mathbf{H}(s, \mathbf{x}^{(n)}) \mathbf{H}(s, \mathbf{x}^{(k)}) \delta a(s) \, ds. \qquad (B22)$$

41

Acknowledgements

References

Ashby, M.F., Blunt F.J., and Bannister, M., (1989), "Flow characteristics of highly constrained metal wires," *Acta Metallurgica*, **37**, pp.1847–1857.

Aveston, J. and Kelly, A. (1973), "Theory of multiple fracture in fibrous composites," *Journal of Materials Science*, **8**, pp.352–362.

Ballarini, R., Shah, S.P. and Keer, L.M., (1984), "Crack growth in cement based composites," *Engineering Fracutre Mechanics*, **20**(3), pp.433–445.

Bower, A.F. and Ortiz, M., (1990), "Solution of three–dimensional crack problems by a finite perturbation method," to appear in *Journal of the Mechanics and Physics of Solids*.

Budiansky, B., (1986), "Micromechanics II," Proc. 10th National U.S. Congress of Applied Mechanics, Austin, Texas, P.J. Lamb (ed), pp.25–32.

Budiansky, B. and Amazigo, J.C., (1989), "Touthening by aligned, frictionally constrained fibres," *Journal of the Mechanics and Physics of Solids*, **37**(1), pp.93–109.

Budiansky, B., Amazigo, J.C. and Evans, A.G., (1988), "Small scale crack bridging and the fracture toughness of particulate reinforced ceramics," *Journal of the Mechanics and Physics of Solids*, **36**(2), pp.167–187.

Budiansky, B., Hutchinson, J. and Evans, A.G., (1986), "Matrix fracture in fibre reinforced ceramics," *Journal of the Mechanics and Physics of Solids*, **34**, pp.167–189.

Charalambides, P.G. and McMeeking, R.M., (1987), "Finite element method simulation of crack propagation in a brittle microcracking solid," *Mechanics of Materials*, **6**, pp.71–87

Claussen, N. (1976), "Fracture toughness of Al_2O_3 with an unstabilized ZrO_2 dispersed phase," *Journal of the Americal Ceramics Society*, **59** pp.49–51.

Evans, A.G., (1972), "The strength of brittle materials containing second phase dispersions," *Philosophical Magazine*, **26**, pp.1327.

Evans, A.G., (1984), "Aspects of the reliability of ceramics," *Defect properties and processing of high-tech nonmetallic materials*, Crawford, J.H., Chen, Y. and Sibley, W.A. (eds), North Holland, pp.63–80.

Evans, A.G. and Faber, K.T., (1981), "Toughening of ceramics by circumferential microcracking," *Journal of the American Ceramics Society*, 64(7), pp.394–398.

Evans, A.G. and Fu, Y., (1985), "Some effects of microcracks on the mechanical properties of brittle solids II: Microcrack toughening," *Acta Metallurgica*, 33, pp.1525–1531.

Evans, A.G., Heuer, A.H. and Porter, D.L., (1977), "The fracture toughness of ceramics," *Advances in research on the strength and fracture of materials, ICF4*, D.M.R. Taplin (ed).

Faber, K.T. and Evans, A.G., (1983), "Crack deflection processes I: Theory," *Acta Metallurgica*, 31(4), pp.565–576

Faber, K.T. and Evans, A.G., (1983), "Crack deflection processes II: Experiment," *Acta Metallurgica*, 31(4), pp.577–584.

Fares, N., (1990), "Crack fronts trapped by arrays of obstacles: numerical solutions based on surface integral representation,", *Journal of Applied Mechanics*, 56, pp.837–843

Gao, H. and Rice, J.R., (1986), "Shear Stress Intensity Factors For a Planar Crack with Slightly Curved Front," *Journal of Applied Mechanics*, 53, pp. 774–778.

Gao, H. and Rice, J.R., (1987), "Somewhat Circular Tensile Cracks," *International Journal of Fracture*, 33, pp. 115–174.

Gao, H. and Rice, J.R., (1990), "A first–order perturbation analysis of crack trapping by arrays of obstacles," *Journal of Applied Mechanics*, 56, pp.828–836

Hannant, D.J., Hughes, D.C. and Kelley, A., (1983), "Toughening of brittle solids with fibres," *Phil. Trans. Roy. Soc. Lond.* , A, 310, pp.175–190.

Hillerborg, A., Modeer, M., Petersson, P.E., (1976), "Analysis of crack formation and crack growth in concrete by means of fracture mechanics and finite elements," *Cement and Concrete Research*, 6, pp.773–382.

Hing, P. and Groves, G.W., (1972), "Strength and fracture toughness of polycrystalline magnesium oxide containing metallic particles and fibres," *Journal of Materials Science*, 7(4), pp.427–434.

Hoagland, R.G. and Embury, J.D., (1980), "A treatment of inelastic deformation around a crack tip due to microcracking," *Journal of the American Ceramics Society*, **63**, pp.404–410.

Hoagland, R.G., Hahn, G.T. and Rosenfield, A.R. (1973), "Influence of microstructure on the fracture propagation in rock," *Rock Mechanics*, **5**, pp.77–106.

Hutchinson, J.W., (1987), "Crack tip shieldig by microcracking in brittle solids," *Acta Metallurgica*, **35**(7), pp.1605–1619.

Kachanov, M., (1986), "On crack–microcrack interactions," *International Journal of Fracture*, **30**, pp.65–72.

Krstic, V.V., Nicholson, P.S. and Hoagland, R.G., (1981), "Toughening of glasses by metallic particles," *Journal of the American Ceramics Society*, **64**(9), pp.499–503

Lange, F.F., (1970), "The interaction of a crack front with a second–phase dispersion," *Philosophical Magazine, "*, **22**, pp.983.

Marshall, D.B. and Cox, B.N., (1985), "Matrix cracking in brittle matrix fibre composites," *Acta Metallurgica*, **33**(11), pp.2013–2021.

McHugh, C.O., Whalen, T.J. and Humenik, M., (1966), "Dispersion strengthened aluminium oxide," *Journal of the American Ceramics Society*, **49**(9), pp.486–491.

Mecholsky, J.J., Freiman, S.W., Rice, R.W., (1976), "Fracture surface analysis of ceramics," *Journal of Materials Science*, **11**, pp.1310–1319.

Mendelson, M.I. and Fine, M.F., (1974), "Enhancement of fracture properties of Wustite by precipitation," *Journal of the American Ceramics Society*, **57**(4), pp.154–159.

Ortiz, M., (1987), "A continuum theory of crack shielding in ceramics," *Journal of Applied Mechanics*, **54**, pp.54–58.

Ortiz, M., (1988), "Microcrack coalescence and macroscopic crack growth initiation in brittle solids," *International Journal of Solids and Structures*, **24**(3), pp.231–250.

Ortiz, M. and Giannakopoulos, A., (1989), "Mixed mode crack tip fields in monolithic ceramics," *International Journal of Solids and Structures*, in press.

Ortiz, M. and Giannakopoulos, A., (1989) "Maximal crack–tip shielding by microcracking," *Journal of Applied Mechanics*, **56**, pp.297–283.

Ortiz, M. and Giannakopoulos, A.E., "Crack propagation in monolithic ceramics under mixed mode loading," *International Journal of Fracture*, in press.

Ortiz, M. and Molinari, A. (1988), "Microstructural thermal stresses in ceramic materials," *Journal of the Mechanics and Physics of Solids*, **36**, pp.385–400

Ortiz, M. and Suresh, S., (1990), "Residual stresses in ceramics due to thermal and elastic anisotropy: statistical properties and microfracture," submitted for publication.

Rice, J.R., (1985), "First Order Variation in Elastic Fields due to Variation in Location of a Planar Crack Front," *Journal of Applied Mechanics*, **52**, pp. 571–579.

Rice, J.R., (1985), "Three dimensional elastic crack tip interactions with transformation strains and dislocations," *International Journal of Solids and Structures*, **21**, pp.781–791.

Rice, J.R., (1987), "Weight Function Theory for Three–Dimensional Elastic Crack Analysis," To appear in Fracture Mechanics: Perspectives and Directions (Twentieth Symposium), eds. R.P. Wei and R.P. Gangloff, ASTM–STP–1020, American Society Testing and Materials, Philadelphia.

Rodin, G., (1987), "An example of crack tip analysis in brittle damaged materials," *International Journal of Fracture*, **33**, pp.31–35.

Rose, L.R.F., (1975), "Toughening due to crack front interaction with a second phase dispersion," *Mechanics of Materials*, **6**, pp.11-15.

Rose, L.R.F., (1987), "Crack reinforcement by distributed springs," *Journal of the Mechanics and Physics of Solids*, **35**(4), pp.383–405.

Sigl, L.S. and Evans, A.G., (1989), "Effects of residual stress and frictional sliding on cracking and pull out in brittle matrix composites," *Mechanics of Materials*, **8**, pp.1–12.

Suresh, S. (1985), "Fatigue crack deflection and fracture surface contact: micromechanical models," *Metallurgical Transactions*, **16A**, pp.249–260.

Swanson, P.L., Fairbanks, C.J., Lawn, B.R., Mai, Y.W. and Hockey, B.J., (1987), "Crack interface grain bridging as a fracture resistance mechanism in ceramics I: Experimental study on alumina," *Journal of the American Ceramics Society*, **70**(4), pp.279-289.

Ulfyand, Y.S., (1965), "Survey of articles on the application of integral transforms in theory of elasticity," University of North Carolina, Raleigh, N.C.

Vekinis, G., Ashby, M.F. and Beaumont, P.W.R., (1990), "R–curve behaviour of Al_2O_3 ceramics," To appear in Acta Metallurgica.

Velazco, G., Visalvanich, K. and Shah, S.P., (1980), "Fracture behaviour of fibre reinforced beams," *Cement and Concrete Research*, **10**, pp.41-51.

Wecharatana, M. and Shah, S.P., (1982), "A model for predicting fracture resistance in reinforced concrete," *Cement and Concrete research*, **13**, pp.819-829.

Wu, C.C., Frieman, S.W., Rice, R.W. and Mecholsky, J.J., (1978), "Microstructural aspects of crack propagation in ceramics," *Journal of Materials Science*, **13**, pp.2659-2670.

List of Figures

Fig. 17: Variation of length of bridged zone with frictional energy dissipation. $L^2 \delta_{\text{crit}}/\Lambda R P_0 = 20 \times 10^3$, $\delta_{\text{crit}}/R = 2.0$.

Fig. 18: Variation of length of bridged zone with compliance ratio. $P_0 \delta_{\text{crit}}/\Lambda (K_c^{\text{max}})^2 = 2.0$, $\delta_{\text{crit}}/R = 2.0$.

TABLE 1

Parameters for frictional pull-out model

Shear Modulus μ	124 GNm^{-2}
Poissons Ratio ν	0.21
Inherent toughness K_c^{mat}	1.95 $\text{MNm}^{-3/2}$
Grain Size $2R$	6.0 μm
Height of grain δ_{crit}	6μm
Tough Grain Spacing L	23 μm
Residual stress σ_r	120 MNm^{-2}
Friction Coefficient f	0.6
$P_0 = f\sigma_r\pi R\delta_{\text{crit}}$	0.008 N
$\Lambda = (1-\nu)/\mu$	6.37×10^{-12} m^2N^{-1}
$P_0\delta_{\text{crit}}/L^2\Lambda(K_c^{\text{mat}})^2$	4.2
R/L	0.15
$L^2\delta_{\text{crit}}/\Lambda R P_0$	20×10^3
δ_{crit}/R	2.0

49
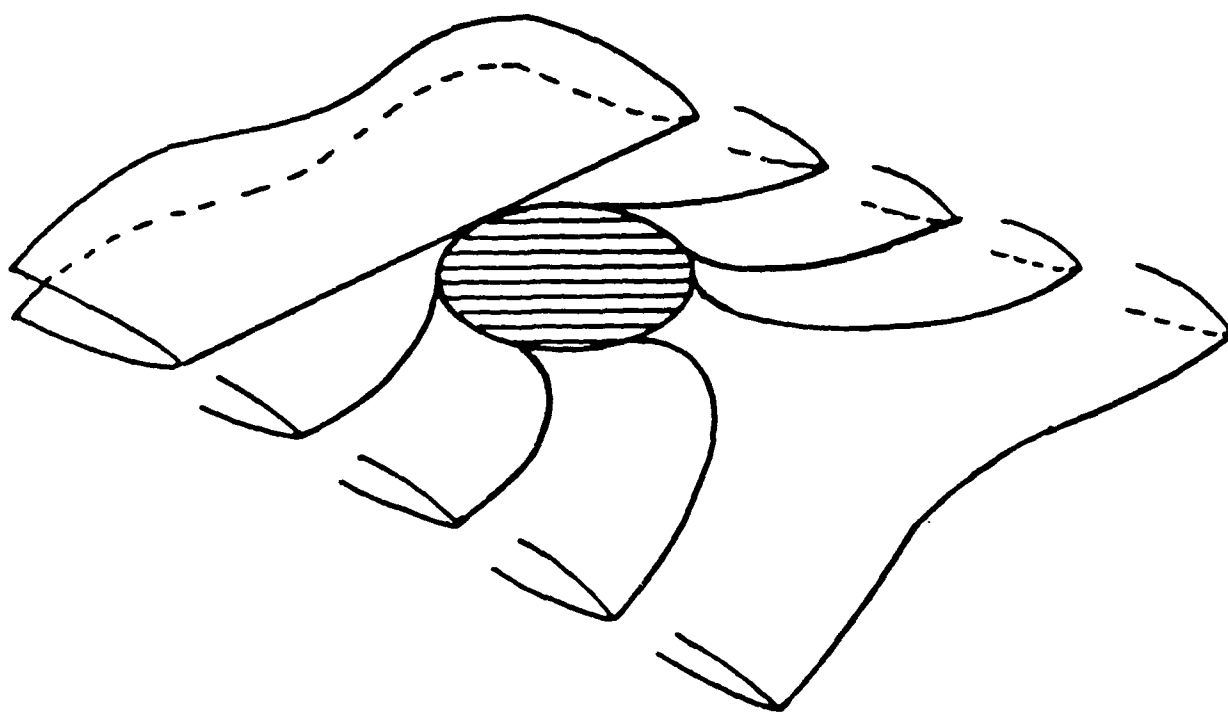
Fig. 1: Mechanism for forming bridging particles in the wake of a
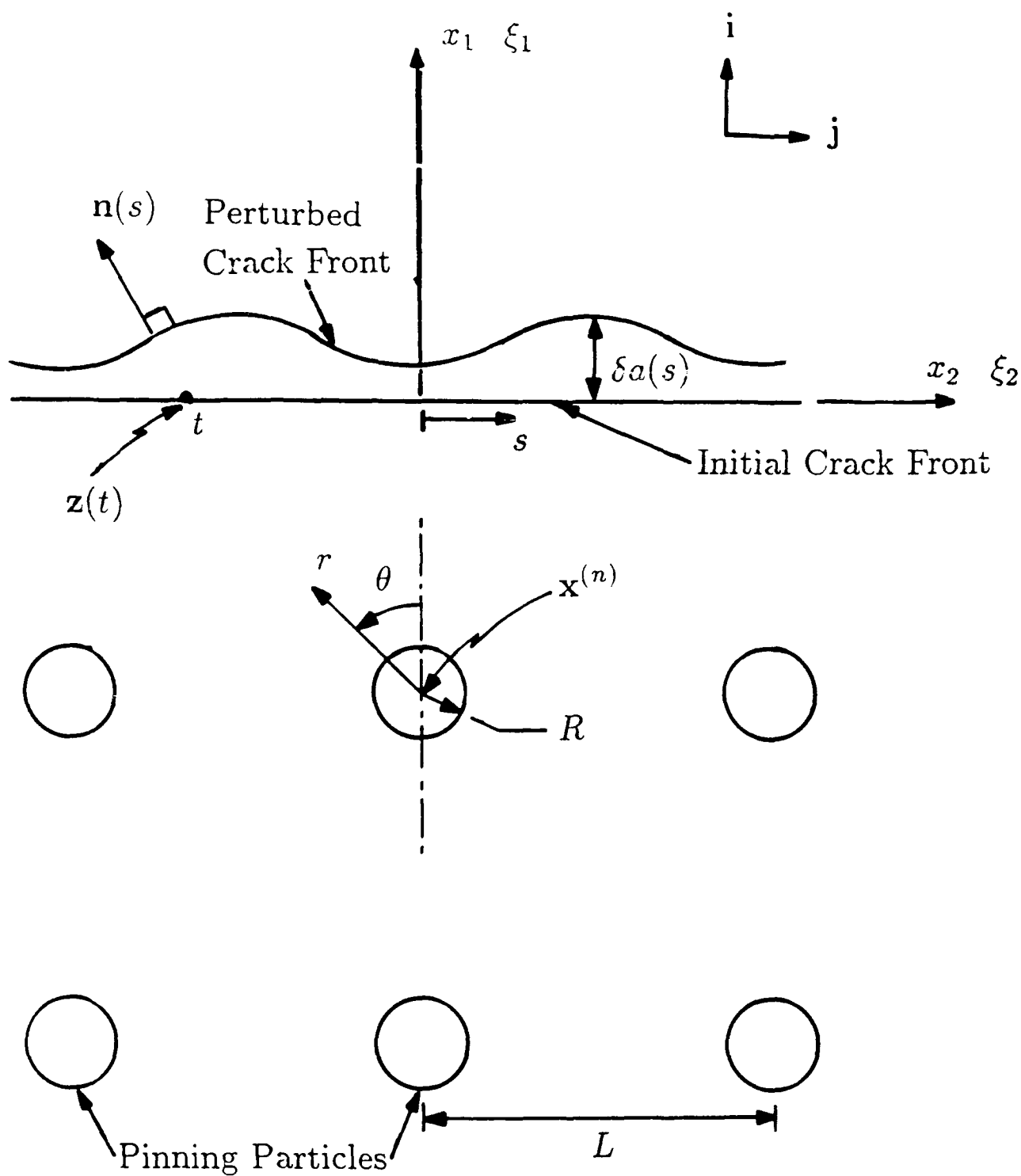crack.

Fig. 2: Semi–infinite crack pinned by parallel rows of obstacles, showing notation and sign convention.
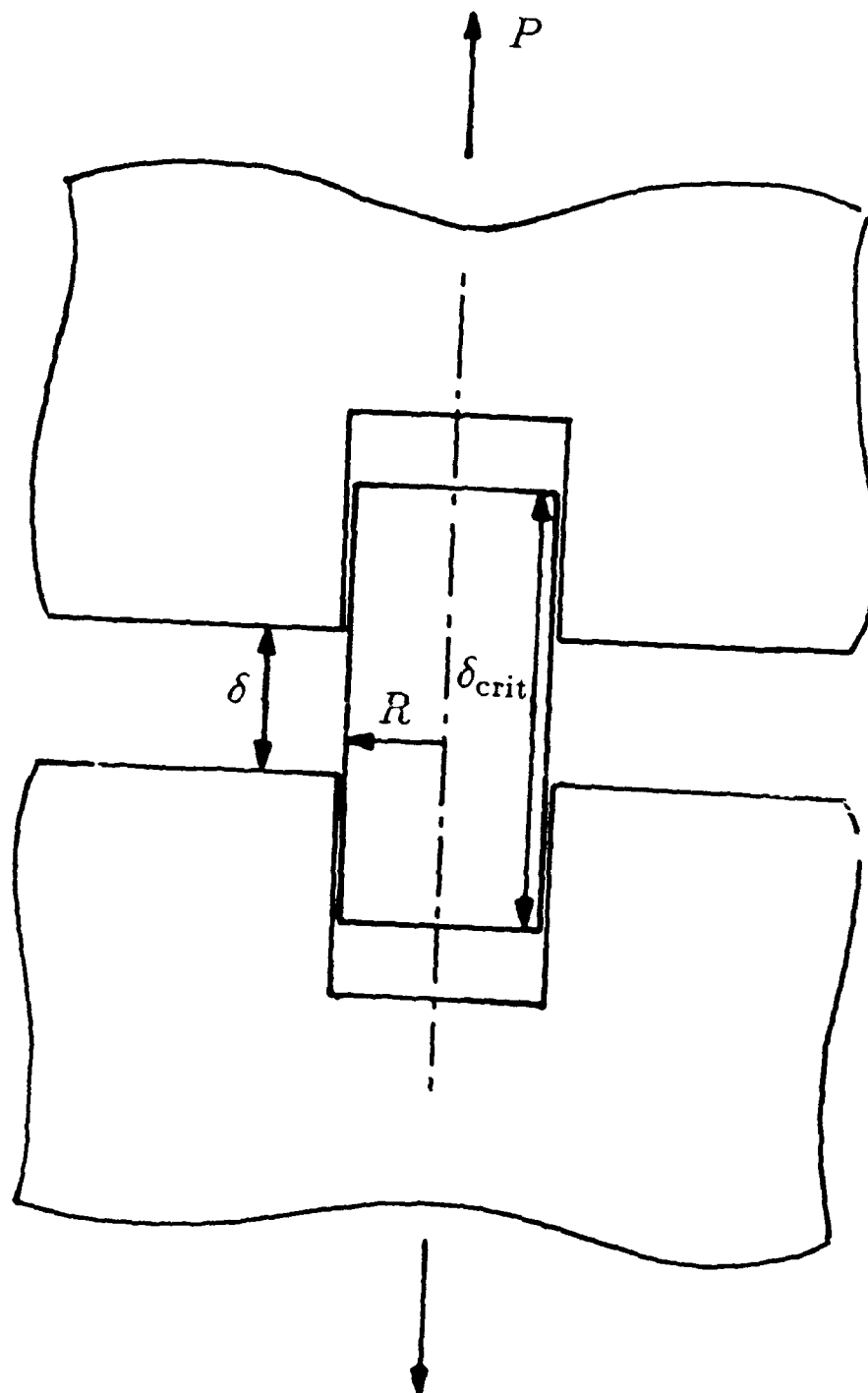
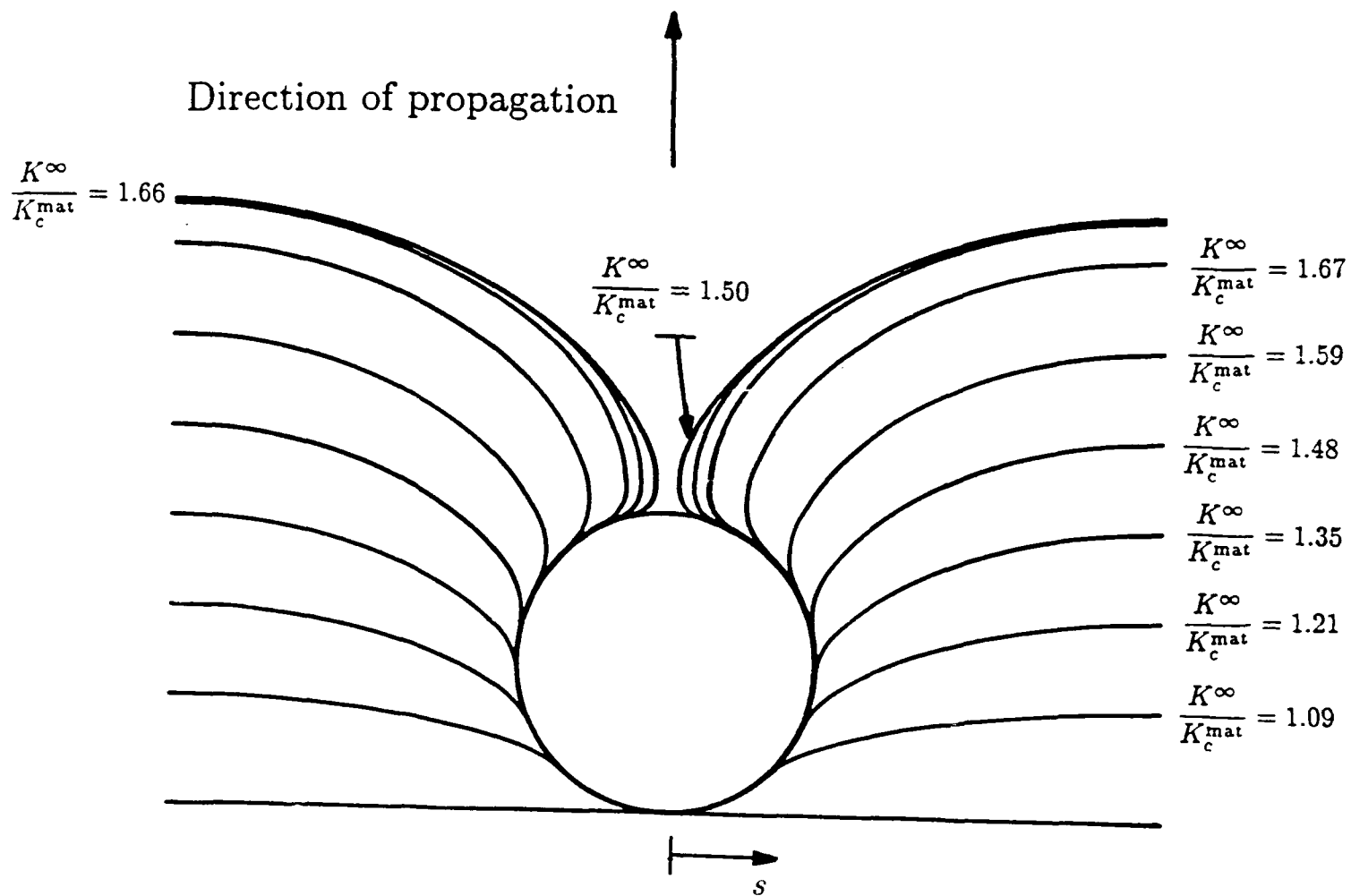Fig. 3: Model of a grain pulling out in the wake of a crack.

Fig. 4: The shape of a semi–infinite crack as it bypasses a single row of obstacles. $L/R = 6.667$.
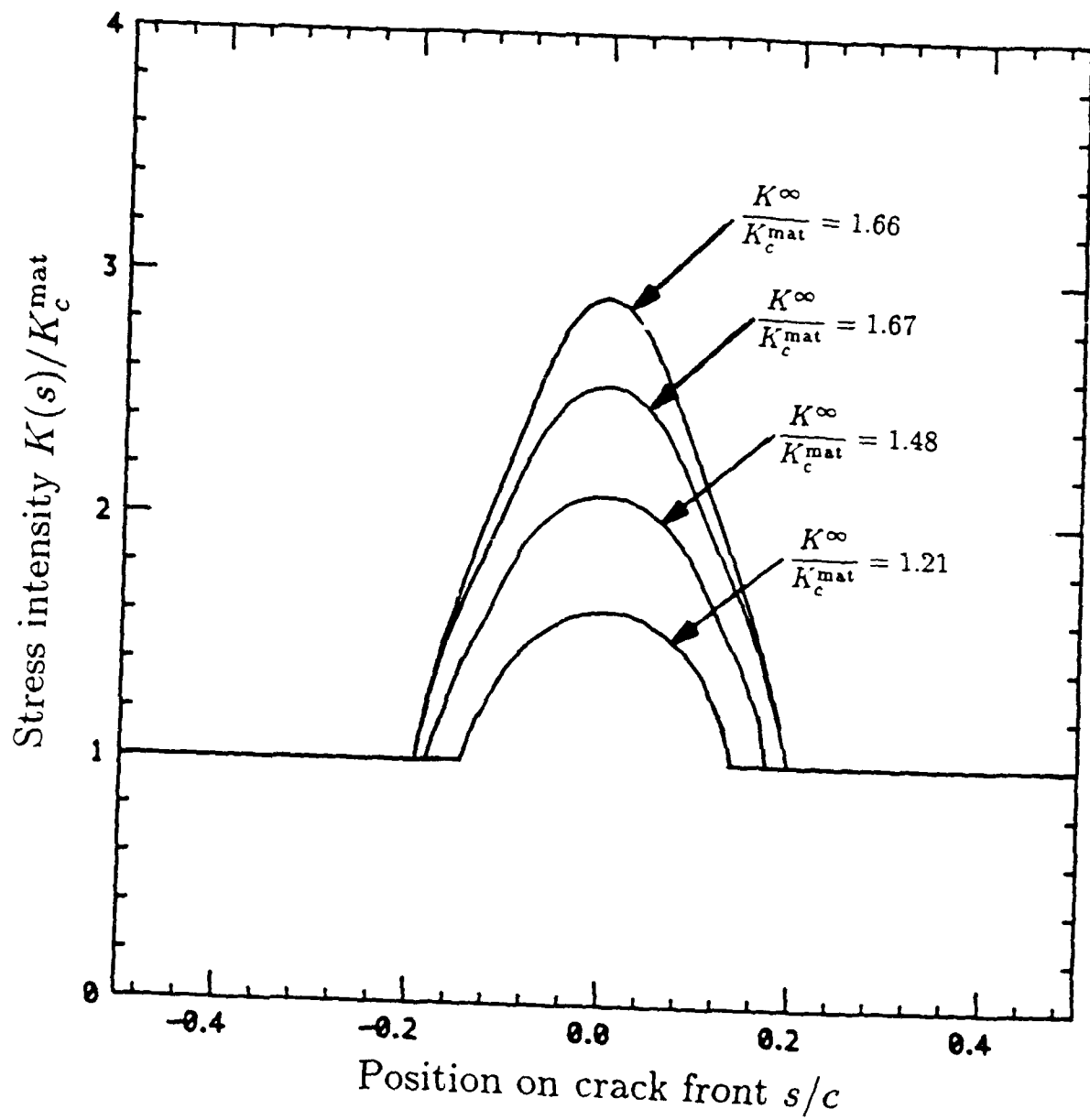
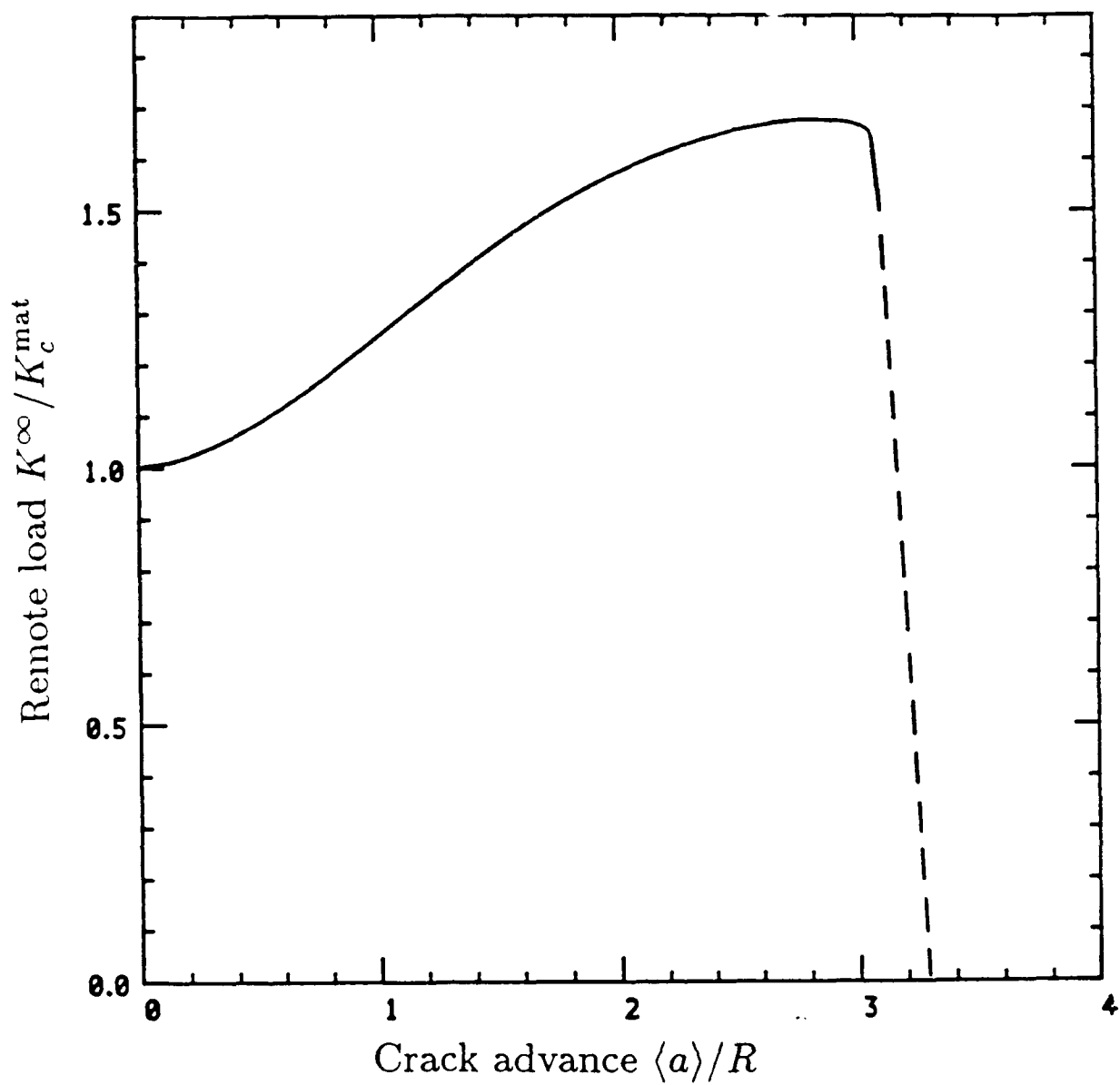Fig. 5: The variation of stress intensity factor around the crack front shown in Fig. 4.

Fig. 6: The variation of remote load with average crack advance
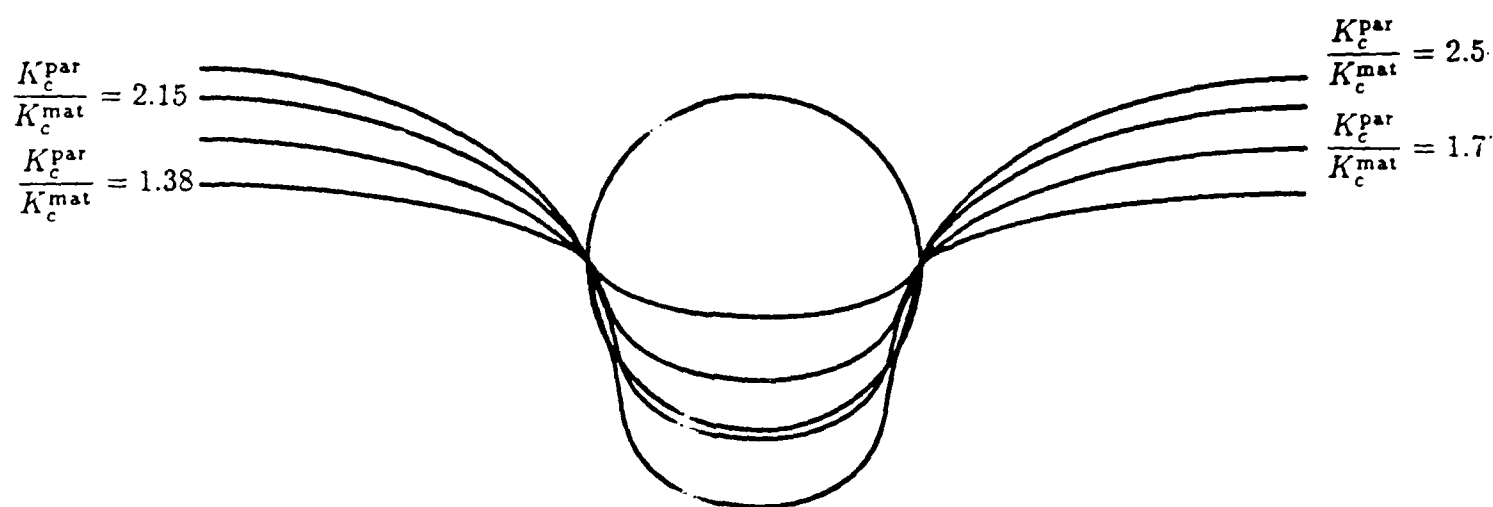for the crack shown in Fig. 4.

Fig. 7: Crack profiles for a fully penetrated particle, for $L/R = 6.667$.

$$\frac{K^\infty}{K_c^{\text{mat}}} = 1.09$$

$$\frac{K^\infty}{K_c^{\text{mat}}} = 1.21$$

$$\frac{K^\infty}{K_c^{\text{mat}}} = 1.34$$

$$\frac{K^\infty}{K_c^{\text{mat}}} = 1.48$$

$$\frac{K^\infty}{K_c^{\text{mat}}} = 1.52$$

$$\frac{K^\infty}{K_c^{\text{mat}}} = 1.53$$

$$\frac{K^\infty}{K_c^{\text{mat}}} = 1.5\zeta$$
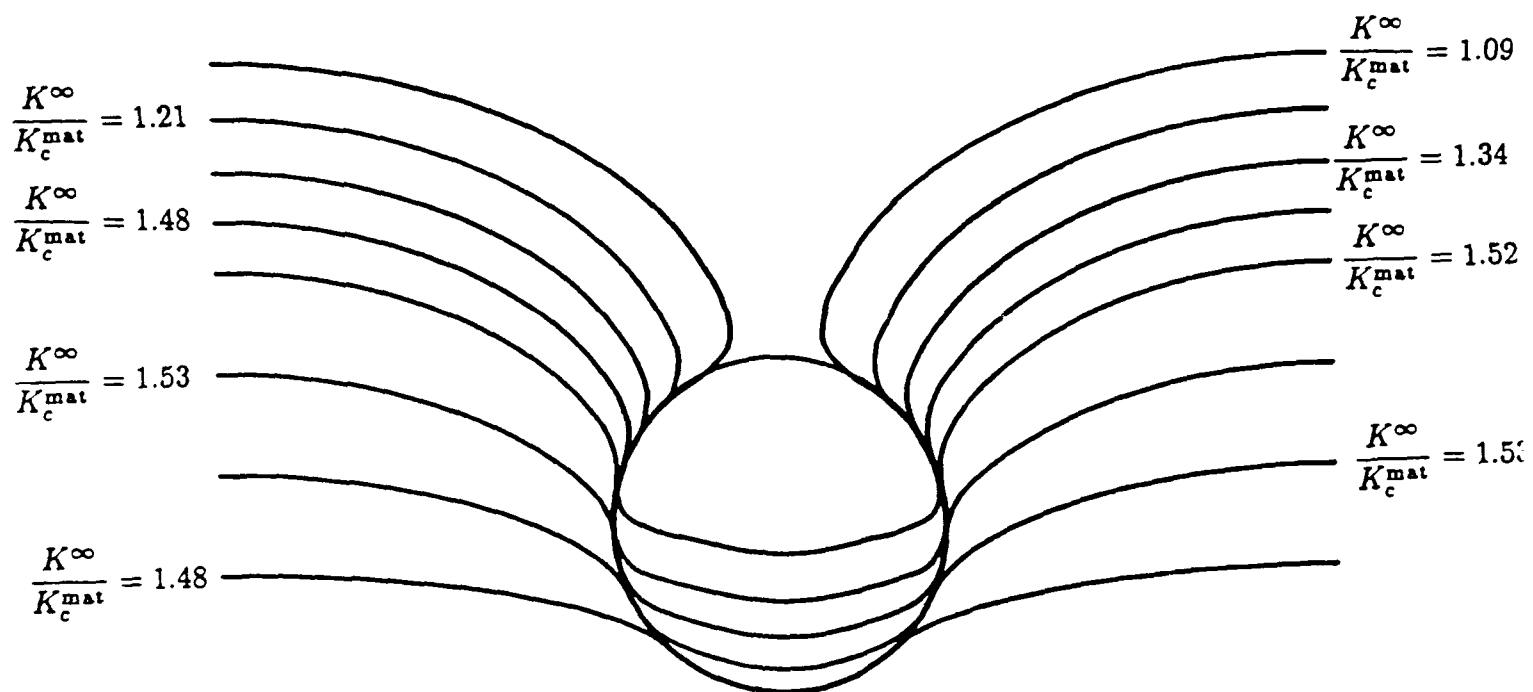
$$\frac{K^\infty}{K_c^{\text{mat}}} = 1.48$$

Fig. 8: Crack profiles during unstable penetration of a particle, for $L/R = 6.667$ and $K_c^{\text{par}}/K_c^{\text{mat}} = 2.4$
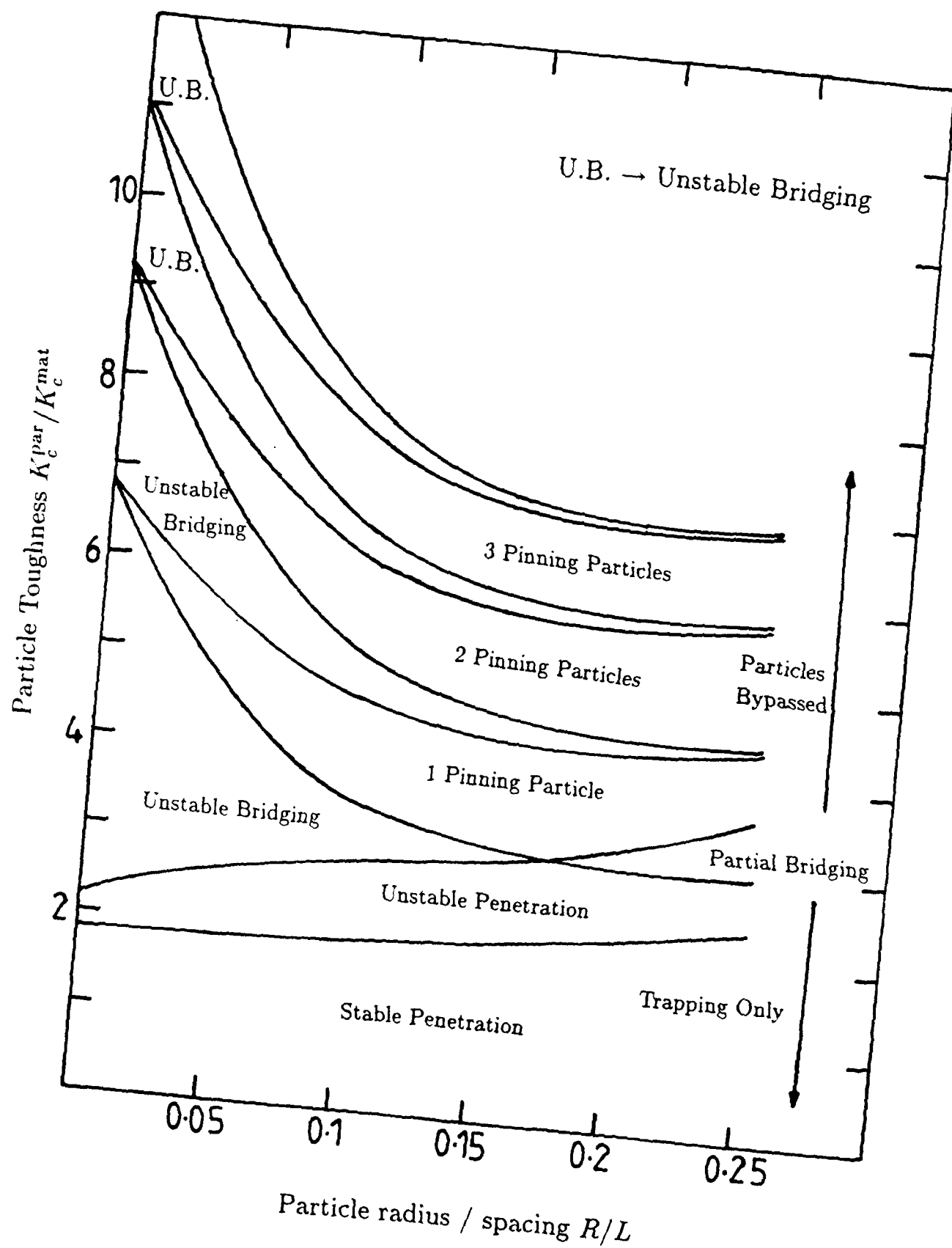
Fig. 9: Regimes of behaviour for a semi-infinite crack propagating through a rectangular array of perfectly pinned particles.
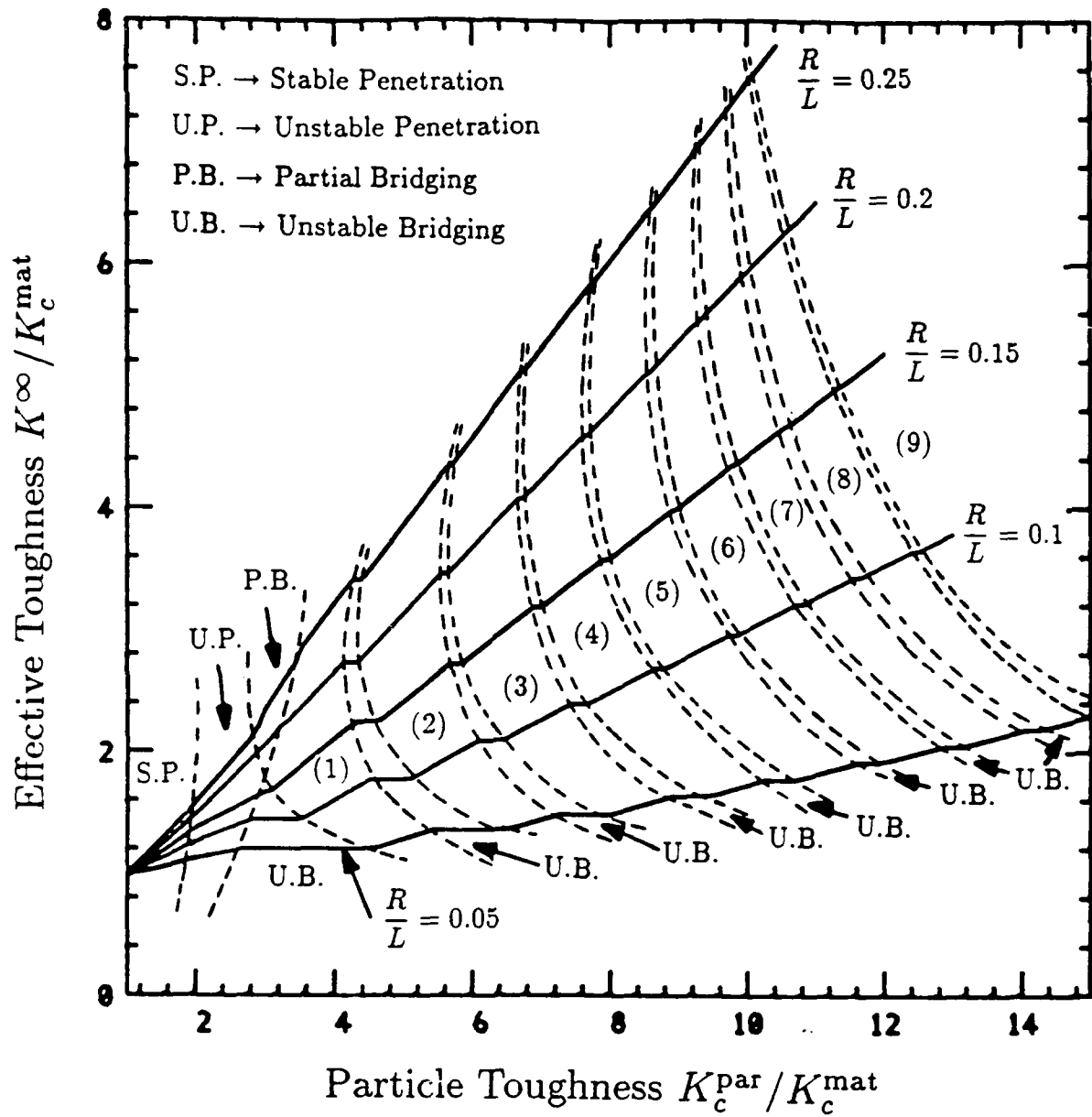
Fig. 10: Effective toughness of a material reinforced by an array of perfectly bonded particles. Numbers in parentheses indicate number of stable pinning particles in the crack wake.

$$\frac{K^\infty}{K_c^{mat}} = 2.41$$

$$\frac{K^\infty}{K_c^{mat}} = 2.38$$

$$\frac{K^\infty}{K_c^{mat}} = 2.20$$

$$\frac{K^\infty}{K_c^{mat}} = 2.00$$

$$\frac{K^\infty}{K_c^{mat}} = 2.31$$

$$\frac{K^\infty}{K_c^{mat}} = 2.10$$

$$\frac{K^\infty}{K_c^{mat}} = 1.91$$

$$\frac{K^\infty}{K_c^{mat}} = 1.80$$

$$\frac{K^\infty}{K_c^{mat}} = 1.84$$

$$\frac{K^\infty}{K_c^{mat}} = 1.88$$

$$\frac{K^\infty}{K_c^{mat}} = 2.07$$

$$\frac{K^\infty}{K_c^{mat}} = 1.91$$

$$\frac{K^\infty}{K_c^{mat}} = 1.73$$

$$\frac{K^\infty}{K_c^{mat}} = 1.59$$

$$\frac{K^\infty}{K_c^{mat}} = 2.10$$

$$\frac{K^\infty}{K_c^{mat}} = 2.01$$

$$\frac{K^\infty}{K_c^{mat}} = 1.82$$

$$\frac{K^\infty}{K_c^{mat}} = 1.65$$

$$\frac{K^\infty}{K_c^{mat}} = 1.55$$

$$\frac{K^\infty}{K_c^{mat}} = 1.57$$

$$\frac{K^\infty}{K_c^{mat}} = 1.60$$

$$\frac{K^\infty}{K_c^{mat}} = 1.78$$

$$\frac{K^\infty}{K_c^{mat}} = 1.69$$

$$\frac{K^\infty}{K_c^{mat}} = 1.53$$

$$\frac{K^\infty}{K_c^{mat}} = 1.37$$

$$\frac{K^\infty}{K_c^{mat}} = 1.75$$

$$\frac{K^\infty}{K_c^{mat}} = 1.60$$

$$\frac{K^\infty}{K_c^{mat}} = 1.44$$

$$\frac{K^\infty}{K_c^{mat}} = 1.31$$

$$\frac{K^\infty}{K_c^{mat}} = 1.28$$

$$\frac{K^\infty}{K_c^{mat}} = 1.29$$

$$\frac{K^\infty}{K_c^{mat}} = 1.31$$

$$\frac{K^\infty}{K_c^{mat}} = 1.40$$

$$\frac{K^\infty}{K_c^{mat}} = 1.28$$

$$\frac{K^\infty}{K_c^{mat}} = 1.14$$

$$\frac{K^\infty}{K_c^{mat}} = 1.02$$

$$\frac{K^\infty}{K_c^{mat}} = 1.44$$

$$\frac{K^\infty}{K_c^{mat}} = 1.35$$

$$\frac{K^\infty}{K_c^{mat}} = 1.21$$

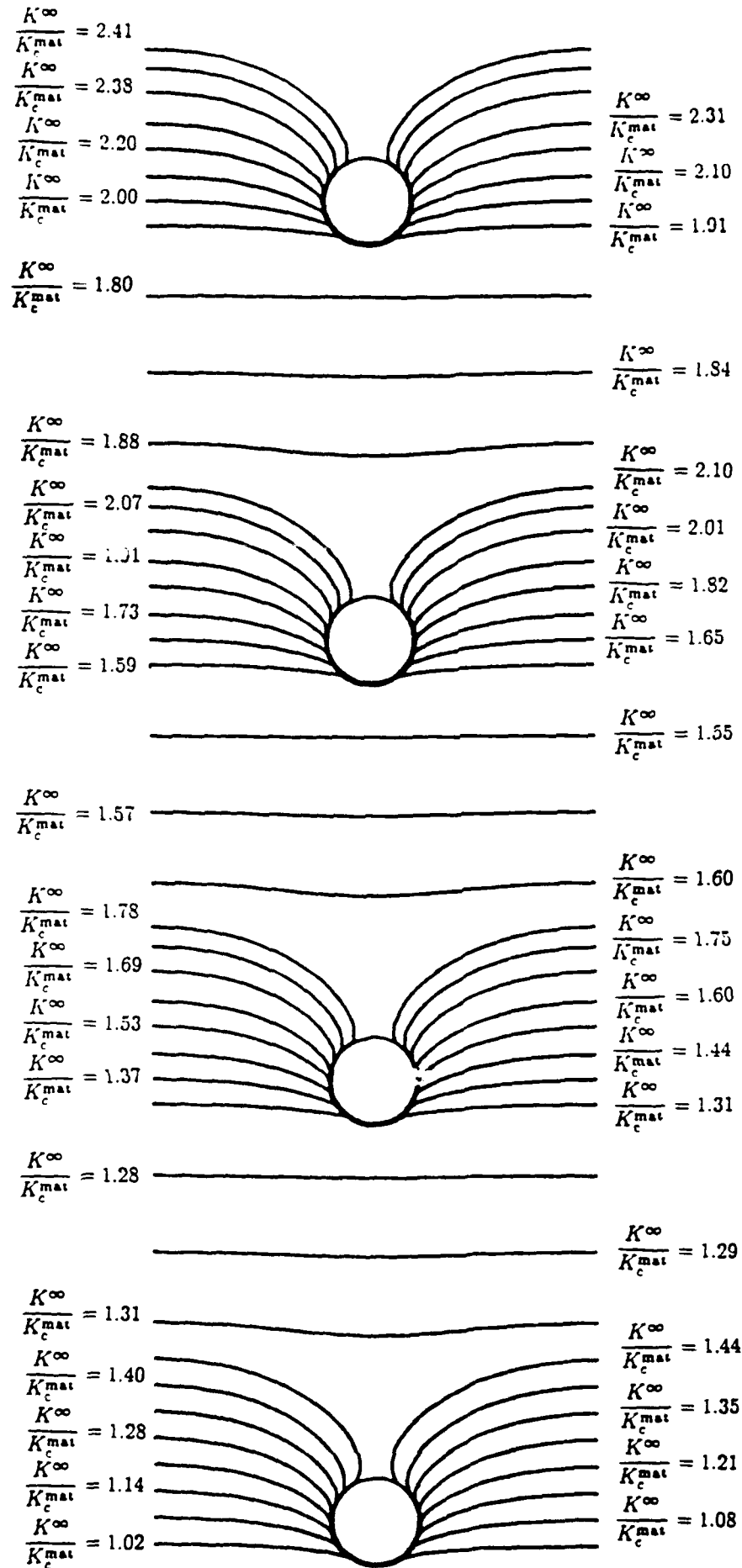$$\frac{K^\infty}{K_c^{mat}} = 1.08$$

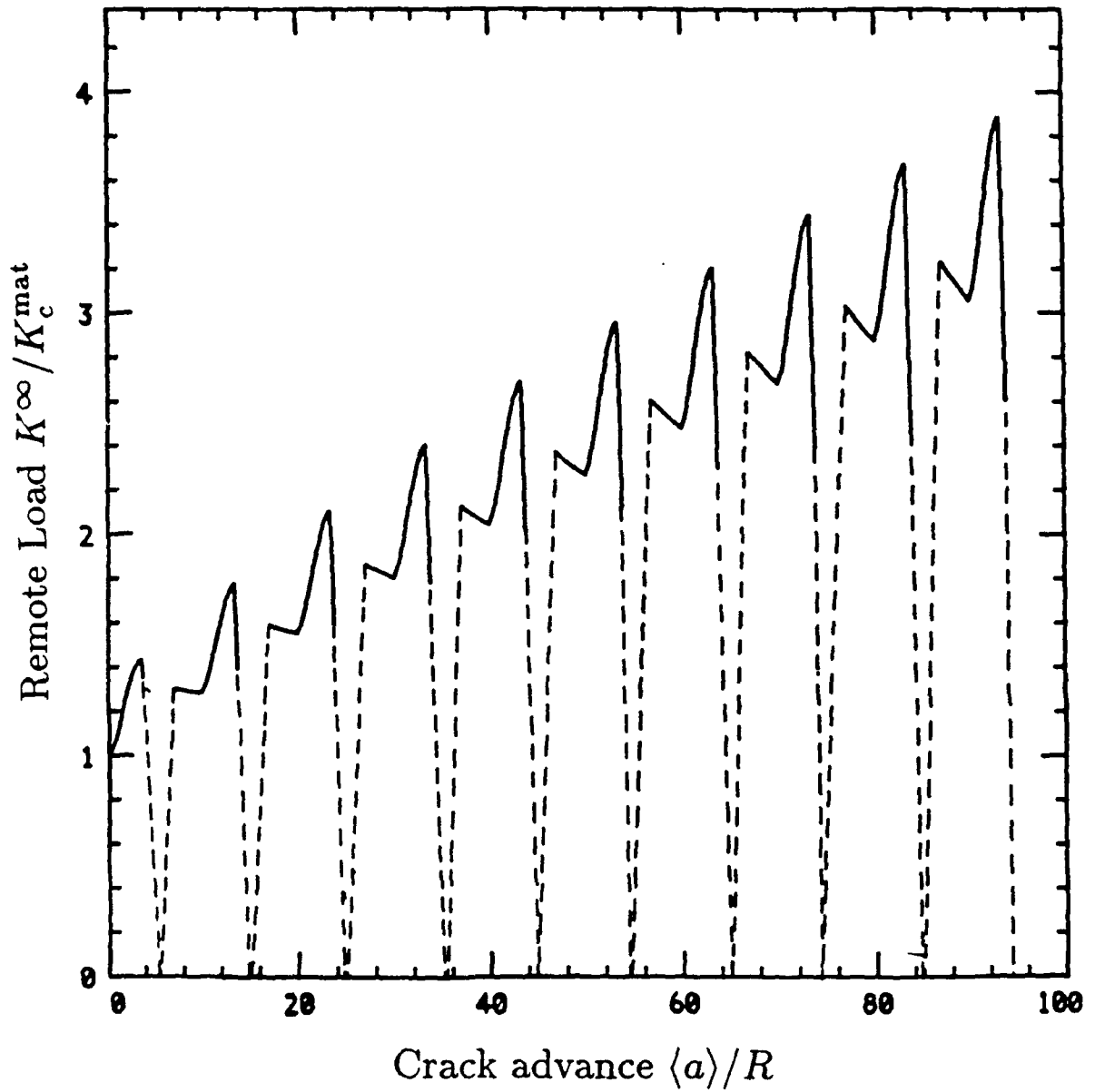Fig. 11: The profile of a semi-infinite crack as it bypasses four suc-

Fig. 12: Variation of load with average crack advance as a semi-infinite crack bypasses 9 rows of perfectly pinned particles. $L/R = 10$.
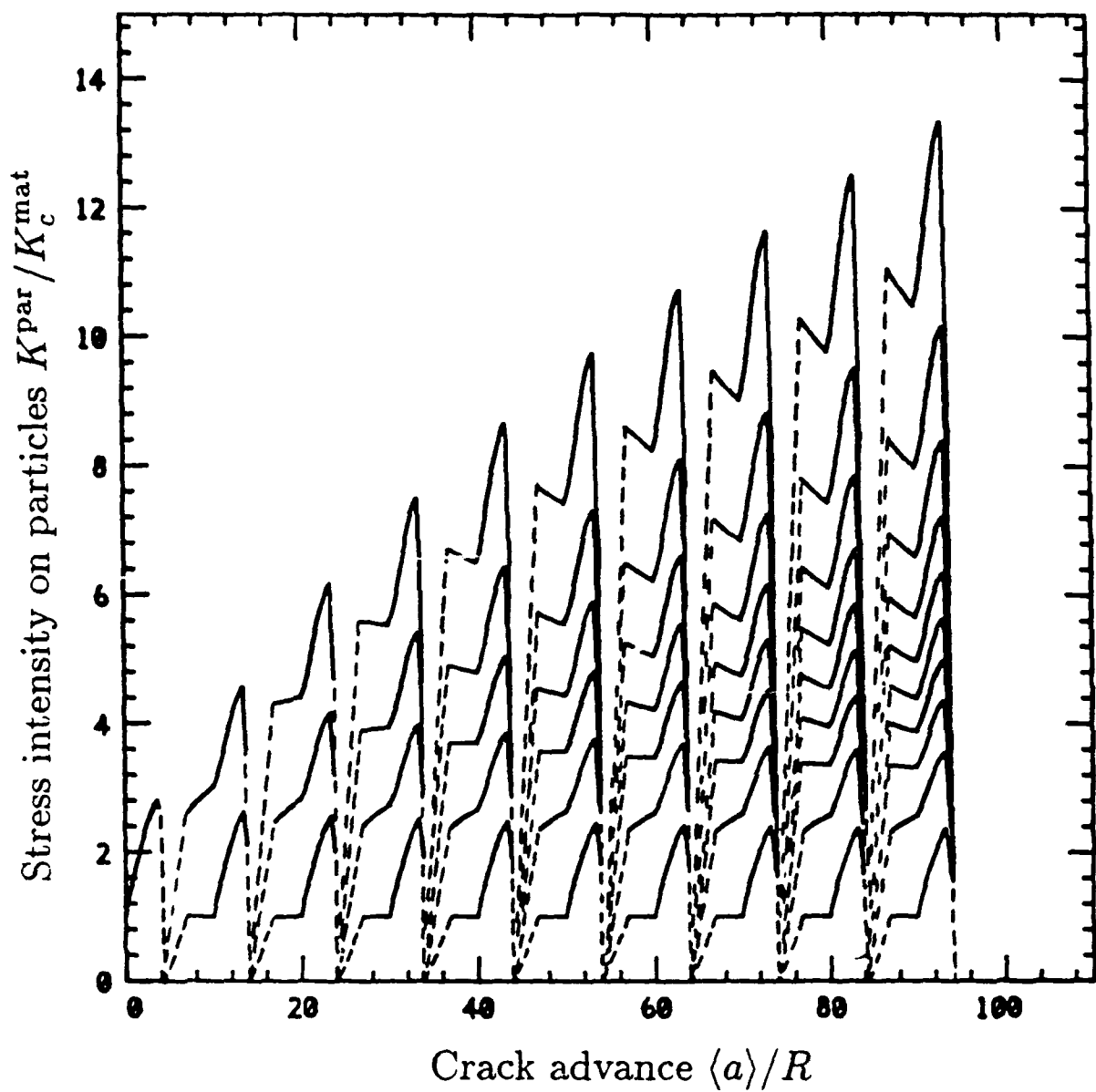
Fig. 13: Variation of stress intensity factors on bridging particles in the wake of a crack, during formation of 9 rows of pinning particles. $L/R = 10$
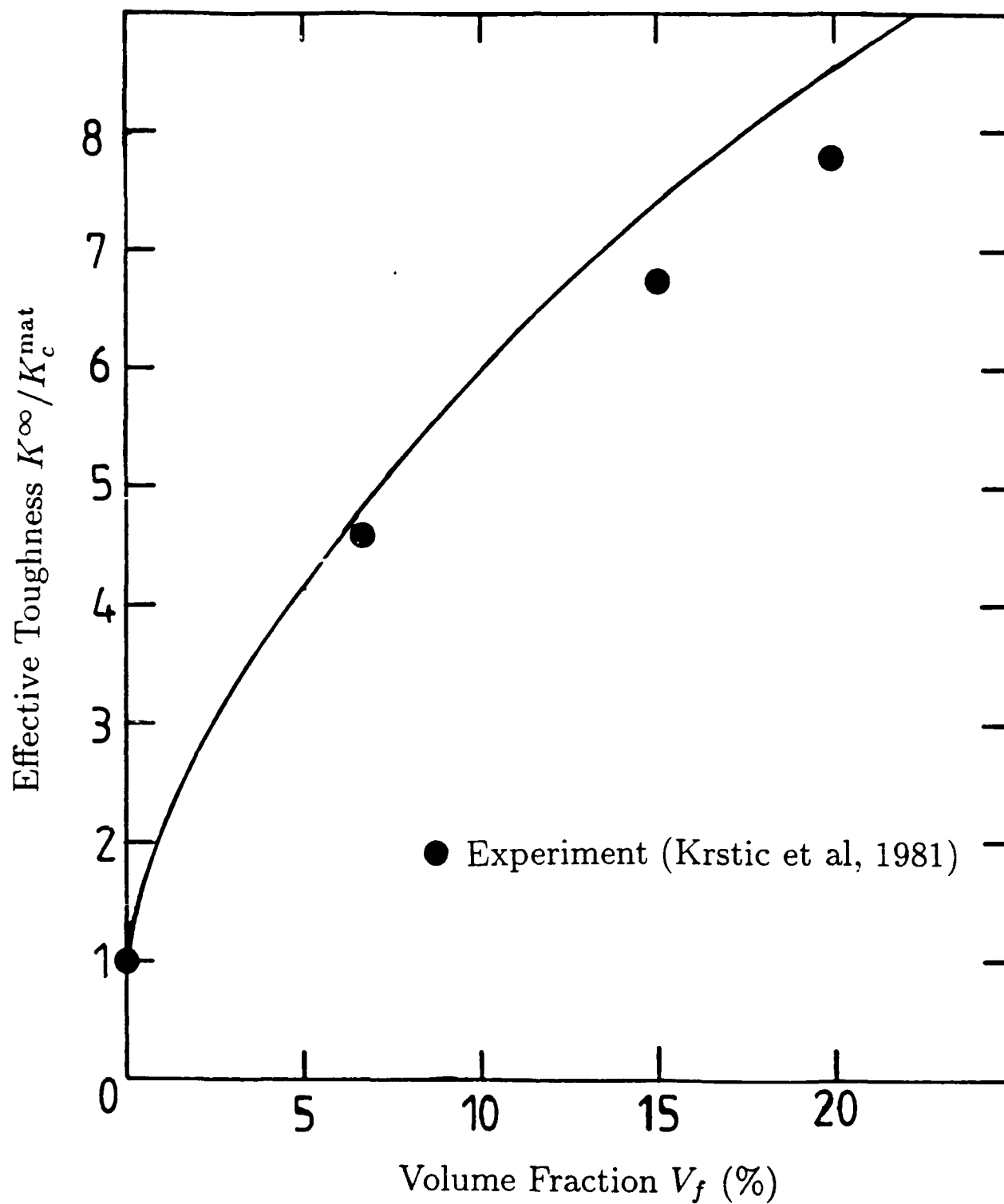
Fig. 14: Comparison of measured and predicted toughness of a brittle matrix reinforced by tough particles. Theory assumes $K_c^{\mathrm{par}}/K_c^{\mathrm{mat}} = 11$.
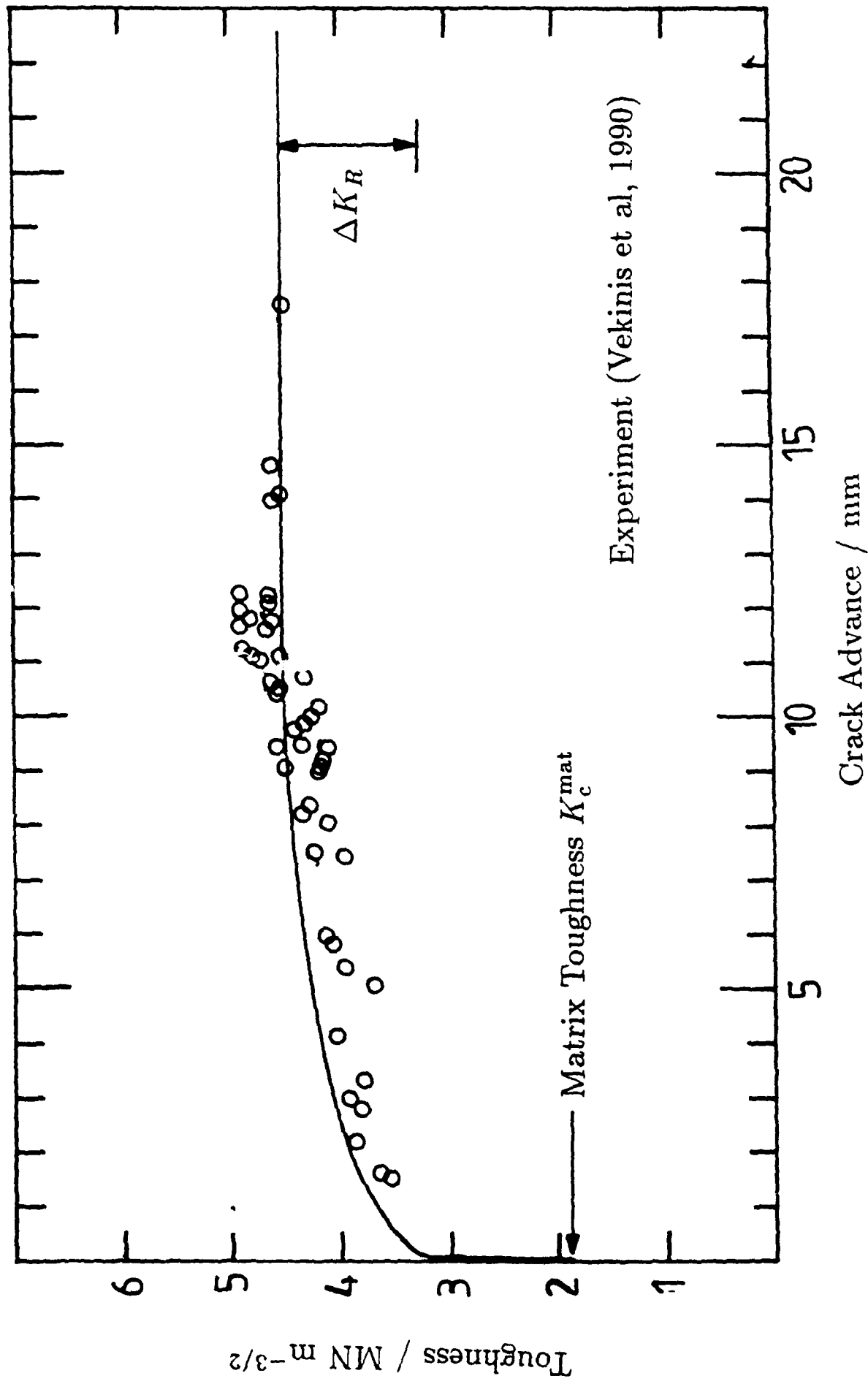
Fig. 15: Comparison of measured and predicted R-curve behaviour for Alumina. Parameters used in the theory are listed in Table 1.
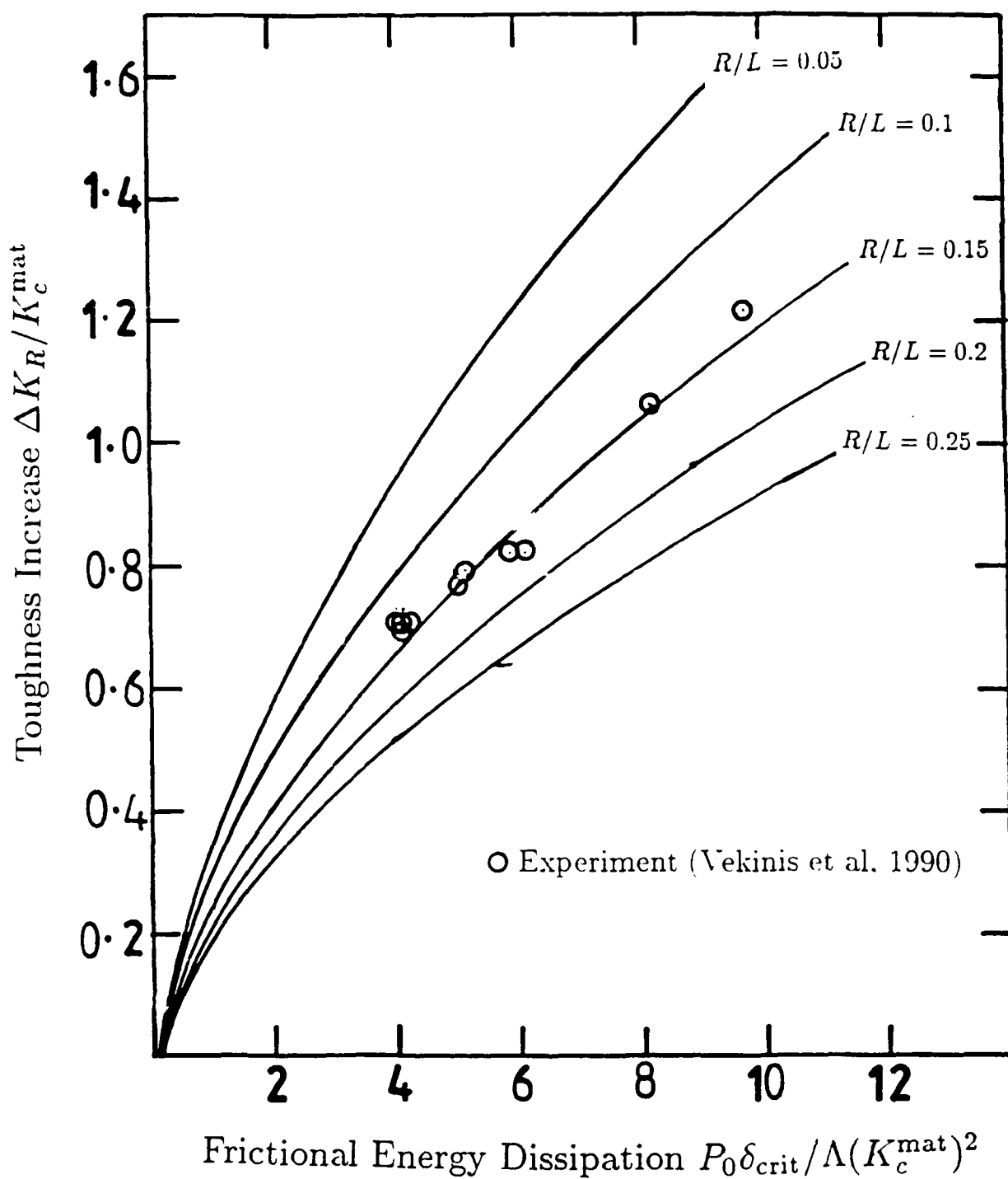
Fig. 16: Variation of toughness enhancement due to frictional bridging with energy dissipation. $L^2 \delta_{crit}/\Lambda R P_0 = 20 \times 10^3$, $\delta_{crit}/R = 2.0$.
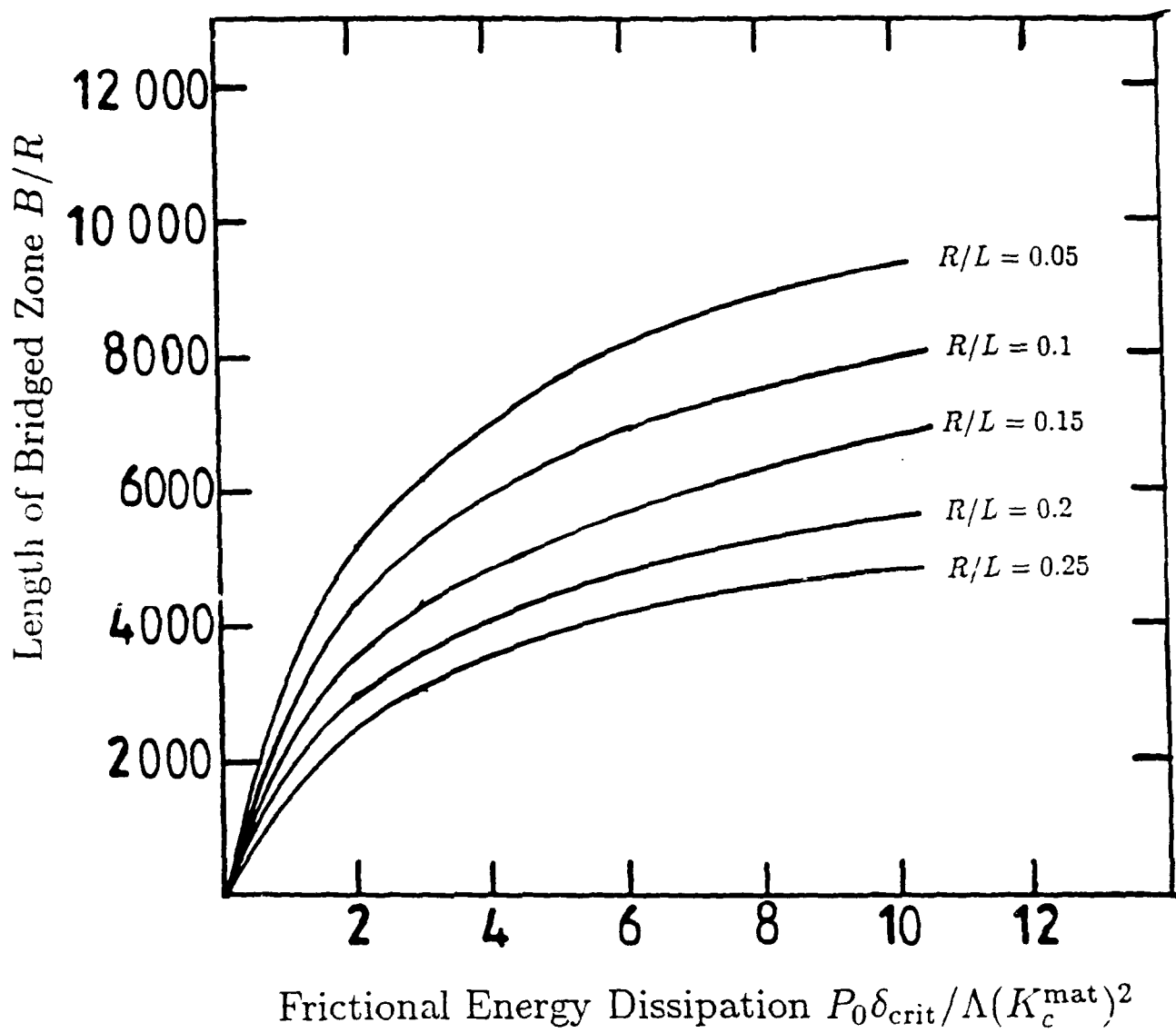
Fig. 17: Variation of length of bridged zone with frictional energy dissipation. $L^2 \delta_{crit}/\Lambda R \Gamma_0 = 20 \times 10^3$, $\delta_{crit}/R = 2.0$.
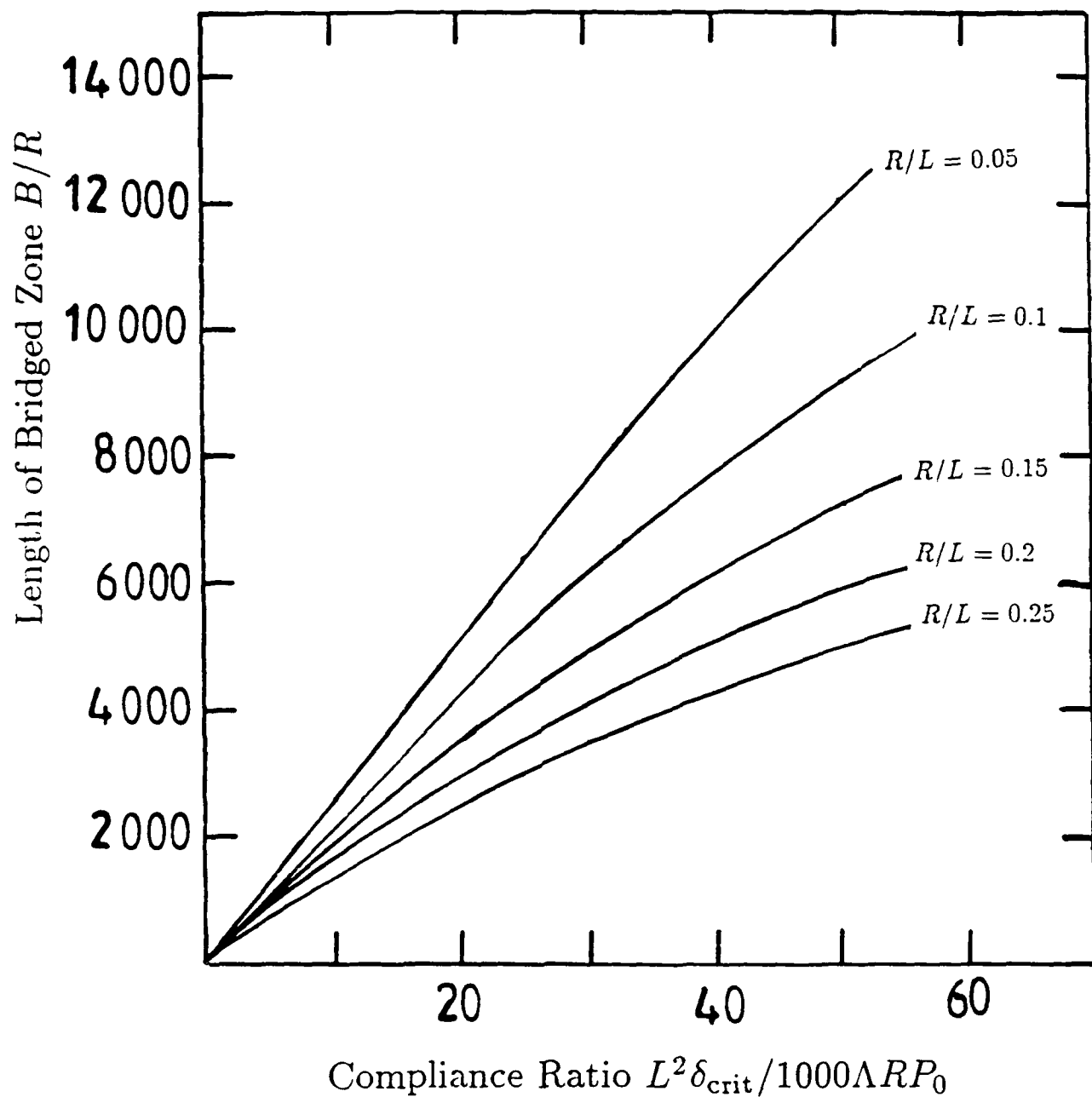
Fig. 18: Variation of length of bridged zone with compliance ratio. $P_0\delta_{\mathrm{crit}}/\Lambda(K_c^{\mathrm{mat}})^2 = 2.0$, $\delta_{\mathrm{crit}}/R = 2.0$.